ANL-76-7

MATERIALS SCIENCE DIVISION
COAL TECHNOLOGY
FOURTH QUARTERLY REPORT,

JULY–SEPTEMBER 1975

U of C-AUA-USERDA

ARGONNE NATIONAL LABORATORY, ARGONNE, ILLINOIS

Prepared for the U. S. ENERGY RESEARCH
AND DEVELOPMENT ADMINISTRATION
under Contract W-31-109-Eng-38

The facilities of Argonne National Laboratory are owned by the United States Government. Under the terms of a contract (W-31-109-Eng-38) between the U. S. Energy Research and Development Administration, Argonne Universities Association and The University of Chicago, the University employs the staff and operates the Laboratory in accordance with policies and programs formulated, approved and reviewed by the Association.

MEMBERS OF ARGONNE UNIVERSITIES ASSOCIATION

The University of Arizona
Carnegie-Mellon University
Case Western Reserve University
The University of Chicago
University of Cincinnati
Illinois Institute of Technology
University of Illinois
Indiana University
Iowa State University
The University of Iowa
Kansas State University
The University of Kansas
Loyola University
Marquette University
Michigan State University
The University of Michigan
University of Minnesota
University of Missouri
Northwestern University
University of Notre Dame
The Ohio State University
Ohio University
The Pennsylvania State University
Purdue University
Saint Louis University
Southern Illinois University
The University of Texas at Austin
Washington University
Wayne State University
The University of Wisconsin

Printed in the United States of America
Available from
National Technical Information Service
U. S. Department of Commerce
5285 Port Royal Road
Springfield, Virginia 22161
Price: Printed Copy $6.50; Microfiche $2.25

Distribution Category:
Coal Conversion and Utilization—
Materials and Components (UC-90h)

ANL-76-7

ARGONNE NATIONAL LABORATORY
9700 South Cass Avenue
Argonne, Illinois 60439

MATERIALS SCIENCE DIVISION
COAL TECHNOLOGY FOURTH QUARTERLY REPORT, JULY—SEPTEMBER 1975

MATERIALS SCIENCE DIVISION

COAL TECHNOLOGY FOURTH QUARTERLY REPORT,

JULY—SEPTEMBER 1975

HIGHLIGHTS

Task A) Evaluation of Ceramic Refractories for Slagging Gasifiers (R. Swaroop)

The cup-slag-corrosion tests were completed using basic slag for 23 refractories up to 1000-h exposure. The refractory systems of the type Al_2O_3 grains with fused bonds, Al_2O_3 grains with chromia solid-solution bonds, and magnesia grains with chromia solid-solution bonds appeared most stable with respect to change in weight and dimensions during their exposure to basic slag at 1445°C. In contrast, the microstructural analysis of slag-exposed tabular alumina with sintered bonds indicated the extensive formation of calcium hexaluminate from the reaction between the tabular Al_2O_3 (grain) and the lime (slag). This resulted in failure of the refractories due to an extensive molar volume increase of the lattice. The refractories that belong to the tabular alumina mullite bond system also appeared to have failed as a result of grain and bond attack by the basic slag.

The cup-slag-corrosion test using acidic slag has been completed up to 500-h exposure for 18 refractories. The microscopic-structural analysis of the exposed specimens has been completed for several grain-bond systems. The utilities hookup to the slag-abrasion-corrosion test rig have been completed without the oxygen line. The preliminary debugging of this rig is in progress.

Task B) Evaluation of Ceramic Coatings for Coal-conversion Plants (R. Swaroop)

The thermal-cycle resistance of the plasma spray coatings of Al_2O_3, $Al_2O_3 \cdot MgO$, ZrO_2 and $MgO \cdot ZrO_2$ was improved with an intermediate layer of bond

coat. Various bond coats were tried. The most effective one which increased the thermal-cycle resistance was observed to be an alloy of Ni-Cr-Al.

The corrosion tests for 20 coating-substrate systems were conducted at 980°C in a coal-gas mixture for a period of 100 h. The coating-substrate systems which survived 100-h exposure were also tested for 500-h exposure. The coatings of zirconia and magnesium zirconates appeared quite promising for protecting the substrates against gaseous attack of the coal-gas mixture. Some alumina-base coatings also indicated medium quality corrosion protection up to 500 h. The coatings of chromium carbide withstood the corrosive environment up to 100 h; however, these coatings disintegrated in 500-h exposure and offered very poor protection to the substrates.

The parts for an erosion-corrosion test apparatus to evaluate ceramic-coated and refractory specimens, at one atmosphere, are being constructed in the ANL machine shop. These are expected to be completed by December 1975.

A multiple-specimen test rig to evaluate the erosion-corrosion behavior of coated specimens is being assembled by Solar Corporation. ANL shipped 54 refractory specimens to Solar in September, 1975. The Kentucky coal char which was sent to Solar about 2 months ago has been analyzed for its chemical composition and the results of this analysis will be forwarded to Solar.

Task C) Nondestructive Testing for Coal Plant Components (W. A. Ellingson)

This past quarter significant results from two field tests at Battelle showed that wall thickness variations on refractory layered structures seem easily detectable by gamma radiography. In addition, gamma radiographs of refractory lined transfer lines have been shown capable of imaging considerable bore detail and may even be useful as an erosion measurement tool. High

temperature wall thickness measurements using ultrasonic delay lines continued with several delay line geometries examined for signal to noise ratios and possible near field effects. Calibration curves have been obtained for the new infrared scanning camera.

Task D) Corrosion Behavior of Materials in Coal-conversion Processes (K. Natesan and O. K. Chopra)

Carburization and oxidation resistance of materials is being evaluated in binary and quarternary gas mixtures consisting of CO, CO_2, CH_4, and H_2. Carburization studies of 100 h duration have been conducted with Ni-base and Fe-base alloys in the carbon activity range from 0.015 to 0.14 at 875°C. Similar experiments at 750 and 1000°C and for time periods of 500 and 1000 h are being initiated.

Task E) Erosion Behavior of Materials in Coal-conversion Processes (M. Mamoun)

During this quarter, major effort has been expended in:

(1) Designing a multi-specimen experimental testing apparatus to investigate the erosive-corrosive behavior of materials used in coal gasifiers;

(2) Extending the developed analytical models so as to include the effects upon metal erosion of the total mass of the eroding particles, the mass flux of the eroding particles, and the angle of impact;

(3) Developing analytical models for material loss by erosion for brittle refractory ceramics;

(4) Establishing analytical criteria for determining the critical conditions leading to material loss by erosion;

(5) Developing computer programs for predicting numerical values for material loss by erosion arising with normal impact.

The analytical results indicate that the erosive resistance of both ductile metals and brittle solids should increase with:

(1) decreasing moduli of elasticity and Poisson's ratios of the eroding particles and the eroded surface,

(2) decreasing mass density of the eroding particles,

(3) increasing yield strength, ultimate strength, and flow stress, or fracture stress of the eroded surface,

(4) the formation of surface films that can effectively reduce the frictional resistance.

Task F) Component Performance and Failure Analysis (S. Greenberg and K. Natesan)

Detailed metallographic examination of failed HYGAS instrument tubing supports the originally stated conclusion that the observed failures were associated with stress corrosion cracking resulting from exposure of Types 304 and 316 stainless steel to steam generated from water containing chloride. Inconel 600 and Incoloy 800 were recommended as more suitable materials. Based on the conclusion that thermocouple sheath failure was caused by internal oxidation, it was recommended that Inconel 702 be replaced with Type 310 stainless steel or nickel-base alloys containing greater than 20% chromium. The stainless steel instrument tubes were replaced with Incoloy 800 and the Inconel 702 thermocouple sheaths with Type 310 stainless steel. These materials performed satisfactorily in a recently completed 370-h run.

Introduction

The present work is being performed by Argonne National Laboratory under Work Order No. 1 of Interagency Agreement No. 1740 issued by the Fossil Energy Division of ERDA. This is the fourth quarterly report* on the six major tasks:

1. Testing and development of ceramic refractories to withstand abrasion-corrosion by coal slag that will be encountered in the Bituminous Coal Research (BCR) Bi-Gas coal-gasification pilot plant;

2. Testing and development of ceramic coatings and refractories for metal parts to increase their resistance to erosion and corrosion in coal-gasification pilot plants;

3. Development, evaluation, and application of nondestructive testing (NDT) methods for use in coal-plant fabrication, construction, and operation to ensure component integrity;

4. Development of models to predict the erosion behavior of components used in coal-gasification plants;

5. Development of models to predict the corrosion behavior of components used in coal-gasification plants; and

6. Analysis of pilot-plant components when failures occur in the operating plant or when components are removed from service.

Progress in each of the six tasks is reported in the sections that follow. The work officially began in October 1974, and this is the fourth quarterly report for the period July through September 1975.*

*Includes work performed during the period June 16 through October 15, 1975.

Task A -- Evaluation of Ceramic Refractories for Slagging Gasifiers
(Principal Investigator: R. Swaroop)

On the basis of refractory applications experience in the steel, glass-forming and petrochemical industries and on conditions that will be produced in coal-slagging gasifiers, the refractories for this program were selected by employing the following criteria: (a) a refractory composition should be chemically stable in an oxygen-steam-char environment to 3200°F; (b) a refractory should be amphoteric to resist chemical attack from acidic and basic slag; and (c) a refractory should have adequate density, mechanical strength, and thermal-shock resistance to withstand the abrasive action of the slag.

In view of the above-mentioned requirements, alumina-base refractories were the primary materials selected for evaluation. The alumina grain is tabular fused or mullite and the bond is either fused, mullite, sintered, calcium-aluminate, phosphate or chromia-solid solution. Also, other refractories that will probably meet these requirements are also being evaluated, i.e., magnesia-grain and silicon carbide (oxide or nitride bonded).

The work for the present quarter has progressed in four directions: (a) cup-slag-corrosion test was completed in basic slag for 23 refractories; (b) cup-slag-corrosion test has been completed in acidic slag up to 500 h; (c) microscopic-structural analysis of the exposed specimens has been completed for certain grain-bond systems; and (d) the utilities hook up to the slag-abrasion-corrosion test rig has been completed and the preliminary debugging of this rig is about to start.

a. Cup-slag-corrosion Test

As described in the second[1] and third[2] quarterly reports, the purpose of the cup-slag-corrosion test is to determine the extent of slag penetration into, and chemical attack of, ceramic refractories at high temperatures in an oxygen-steam environment. The experimental conditions of this test partially simulate

TABLE I. Composition (in Percent) of Various Refractories

Refractory Identification Number*	Al_2O_3	Fe_2O_3	SiO_2	CaO	MgO	TiO_2	$K_2O + Na_2O$	P_2O_5	Cr_2O_3	Si_2ON_2	Si_3N_4	SiC
1 (B)	99-99.5	0.1-0.3	0.2-0.5	0.05-0.15	0.05-0.15	T**	0.1-0.25	-	-	-	-	-
2 (B)	99.3	0.06	0.08	0.13	-	-	0.39	-	-	-	-	-
3 (B)	99.5	0.20	0.15	0.08	0.03	0.01	0.03	-	-	-	-	-
4 (B)	98.7	0.09	0.5	0.5†	-	-	0.03	-	-	-	-	-
5 (B)	95	0.08	4.4	T**	0.01	T**	0.07	-	-	-	-	-
6 (C)	95.4	0.5	2.5	0.04	0.09	-	0.26	1.15	-	-	-	-
7 (C)	95	0.1	0.1	4.6	T**	T**	0.1	-	-	-	-	-
8 (C)	93.7	0.27	0.03	5.4	0.12	T**	0.11	-	-	-	-	-
9 (C)	93.7	0.3	0.1	5.6	0.1	0.1	0.1	-	-	-	-	-
10 (C)	93	0.1	0.2	0.7	-	0.2	0.1	5.6	-	-	-	-
11 (B)	92-94††	0.2	5.0	0.03	0.02	0.21	0.18	-	-	-	-	-
12 (B)	89-91	0.05-0.2	9-11	T**	T**	T**	0.1-0.2	-	-	-	-	-
13 (B)	91.8	0.2	7.7	0.01	0.02	0.1	0.017	-	-	-	-	-
14 (B)	91.6	0.15	8.0	T**	T**	T**	0.15	-	-	-	-	-
15 (B)	90.8	0.2	8.5	0.07	0.07	0.1	0.15	-	-	-	-	-
16 (B)	89.7	0.1	0.05	T**	T**	0.2	0.1	-	10	-	-	-
17 (B)	83.9	1.0	9.0	0.02	0.03	2.3	0.11	-	-	-	-	-
18 (C)	21.4	22.6	2.5	-	9.6	0.6	-	3.7	39.6	-	-	-
19 (B)	16.7	7.8	2.2	0.9	52.8	-	-	-	19.6	-	-	-
20 (B)	13.1	6.8	1.6	0.8	58.7	-	-	-	0.8	-	-	-
21 (B)	13.2	6.3	1.5	0.7	63.8	-	-	-	14.5	-	-	-
22 (B)	4.7	6.1	1.3	-	8.1	-	0.1	-	79.7	-	-	-
23 (B)	90	0.12	0.09	0.05	0.10	0.05	0.05	-	9.5	-	-	-
36 (B)	-	-	-	-	-	-	-	-	-	~70	~20	~10

*(B) is preshaped and (C) is castable. **T: Trace. †May be as B_2O_3. ††As Al_2O_3 and $AlPO_4$.

the operating environment of the first stage of the Bi-Gas gasifier.

Since the last quarterly report,[2] all 24 refractories but one (#36) have completed a 1000-h exposure to basic slag. The chemical compositions of the 24 refractories are given in Table I. The chemical composition of the basic slag is given in Table II. The arrangement of the experimental apparatus has been described earlier.[2]

The cup-slag-corrosion test using acidic slag was initiated and 4-h and 100-h runs were completed. The 1000-h exposure run with fresh slag charge at every 250 h is in progress and a 500-h exposure of some of the specimens has already been completed. The composition of the synthetic acidic slag which is being used for these tests is given in Table II. The basic-to-acidic ratio of the acidic slag varies between 0.71 and 0.73. The melting range of this slag is between 1400 and 1450°C. The experiments are conducted at approximately 1530°C in an oxygen-steam environment. Altogether, 18 refractories are being exposed to the acidic slag. The refractories which have survived 750-h (or more) exposure to basic slag were selected for acidic slag exposure. Refractories which were received from companies during or after the last run for basic slag exposure are also being included in the acidic slag exposure. The compositions of new refractories are given in Table III.

The following can be summarized from the work completed this quarter.

(1) Table IV concludes the observed results for all the refractories (except for #36) which have been exposed to basic slag up to 1000 h. The test on refractory #36 was suspended after 500-h exposure and will be restarted after the completion of acidic slag exposure.

Eight (#2, 4, and 18-23) of the 23 refractories have survived the 1000-h exposure to basic slag without developing any swelling (visible dimensional changes) and/or visible cracks. Refractory #2 has survived a 1000-h [illegible] cracks but has shown swelling at the top of the cup

TABLE II. Compositions of Synthetic Slags*

Components	Wt. % Basic	Wt. % Acidic
SiO_2 (S)	25.6	34-36
Al_2O_3 (A)	13.0	20-21
Fe_2O_3 (F)	12.4	35-37
CaO (C)	27.8	2-2.5
MgO (M)	8.7	2-2.3
TiO_2 (T)	0.4	0.8-1
P_2O_5 (P)	0.9	0.6-1
$(Na_2O + K_2O)$ (M + K)	8	0.2-0.7
SO_3	0.5	0.02-0.04
(Basic/Acidic)+	1.45	0.71-0.73

*From three chemical analyses.

+Basic/Acidic = $\frac{F+C+M+N+K}{S+A+T}$.

TABLE III. Compositions (in wt.%) of New Refractories

Refractory Identification No.	Al_2O_3	SiO_2	CaO	MgO	TiO_2	K_2O + Na_2O	P_2O_5	Cr_2O_3	Fe_2O_3	Others
24 (B)	97.6	<0.1	1.5	-	-	0.4	-	-	<0.1	0.2*
25 (B)	99.5	0.07	-	-	-	0.25	-	-	0.09	0.04
201 (CA)	Fused mullite grain bonded with solid phosphate bond									

*As flourides.

TABLE IV. Cup Slag-corrosion Tests (with Basic Slag).

Refractory Identification Number*	1000-h Run			
	Specimen Condition After			
	250 h	500 h	750 h	1000 h
1 (B)	P, C(S), S	P,C,T		
2 (B)	P(S)	P, S(S)	P,S	P,S
3 (B)	P, C(S), S(S)	P,S,C,T		
4 (B)	P(S)	P	P	P**
5 (B)	P	P,C,T		
6 (CA)	P, C(S)	P,C,T		
7† (CA)	P, C(S), T			
8† (CA)	P,S	P,C,T		
9† (CA)	P,S, C(S)	P,C,T		
10† (CA)	P, C(S), T			
11 (B)	P	P,C,T		
12 (B)	P(S)	P	P,C,T	
13 (B)	P	P,C,S,T		
14 (B)	P(S)	P,C,T		
15 (B)	P	P,C,T		
16 (B)	P(S)	P	P,C,T	
17 (B)	P	P	P,C,T	
18 (CA)	P	P	P	P††
19 (B)	P(thru walls)	P	P	P§
20 (B)	P(thru walls)	P	P	P§
21 (B)	P(thru walls)	P	P	P
22 (B)	P(thru walls)	P	P	P
23 (B)	P	P, S(S)	P,S,C,T	
36 (B)	P, Sh	P, Sh		

(B): Brick or shaped form.
(CA): Castable.
P: Visible penetration or chemical attack.
C: Visible cracks.
(S): Slight or small.
S: Swollen.
Sh: Shrunk or evaporated.
T: Terminated (if severe cracks appeared) except for 21 and 22.

*For chemical composition, refer to Table I.
**Did not crack up to 1559 h; slight swelling at the top.
†Castable dried to 250°F.
††Did not crack or swell up to 1552 h; matrix started crumbling after 1000 h.
§Did not crack or swell up to 1310 h.

(as was shown in Fig. 2, ref. 2). Figures 1 through 3 show the cross sections of refractory specimens #21, 22, and 23, respectively. It is apparent from these pictures that these refractories did not develop visible cracks or swelling. The grain-bond system for these refractories is listed in the figures as well as in Table V. This table also includes the grain-bond systems for other refractories which have survived 750-h (or more) exposure to the basic slag. It should be noticed that fused bond and solid solution bond (especially chromia) have given excellent results with respect to basic slag exposure.

The degradation of refractories with time during their exposure to slag was also recorded by measuring dimensional change and change in weight before, during, and after the slag exposure. The dimensional measurements were taken at the top and bottom of the specimen. The change in weight refers to the difference in weight recorded for a refractory cup with lid (or cover) before and after the test. The recorded data for refractories which survived $\geq$750 h (except #17) are given in Table VI. Refractories 4, 19, 20, 22, and 23 have exhibited long-time dimensional stability. Refractories 2 and 23 indicated slight swelling in the later hours of exposure and refractories 19 and 20 showed slight shrinkage, which is attributed to minor evaporation of matrix or the chemical product(s) that have formed between the slag and the refractory. Refractory 18 has also shown dimensional stability, with a slight loss in weight. This loss in weight is probably the result of a slight disintegration of the refractory matrix after long-time exposure. All other refractories, except #36, exhibited a gain in weight. This gain may be expected if the product formed by the reaction between the refractory and the slag has also accumulated (or reacted with) environmental gases. Refractory #36 has lost weight and reduced in overall size, probably as a result of the slow oxidation of silicon nitride in the oxidizing environment.

(2) All of the 14 refractories evaluated for acidic slag-cup test indicated apparent chemical attack by slag within 4.5- and 100-h exposures.

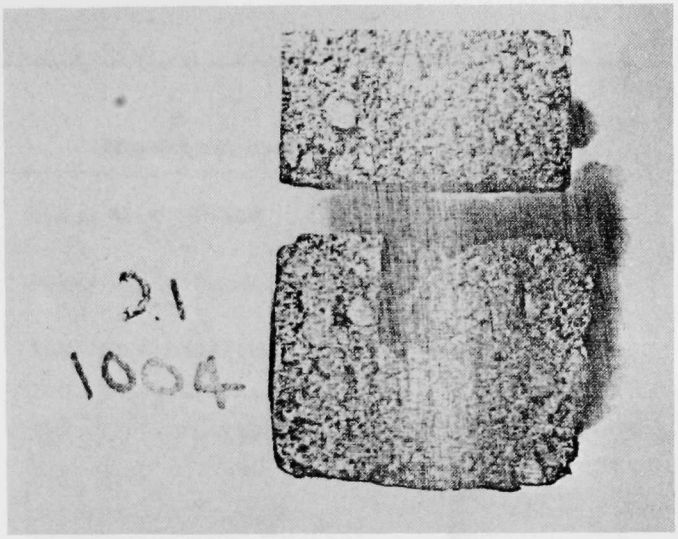

Fig. 1. Refractory #21 which Survived 1004 h of Basic Slag Exposure.

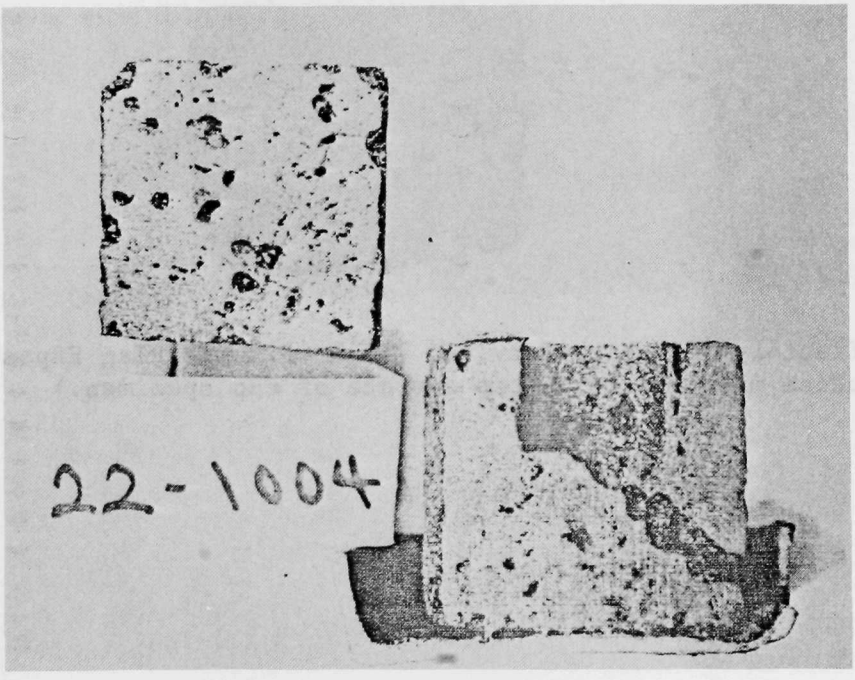

Fig. 2. Refractory #22 which Survived 1004 h of Basic Slag Exposure. (Notice slag channel developed through the pores; could be an original defect of the specimen.)

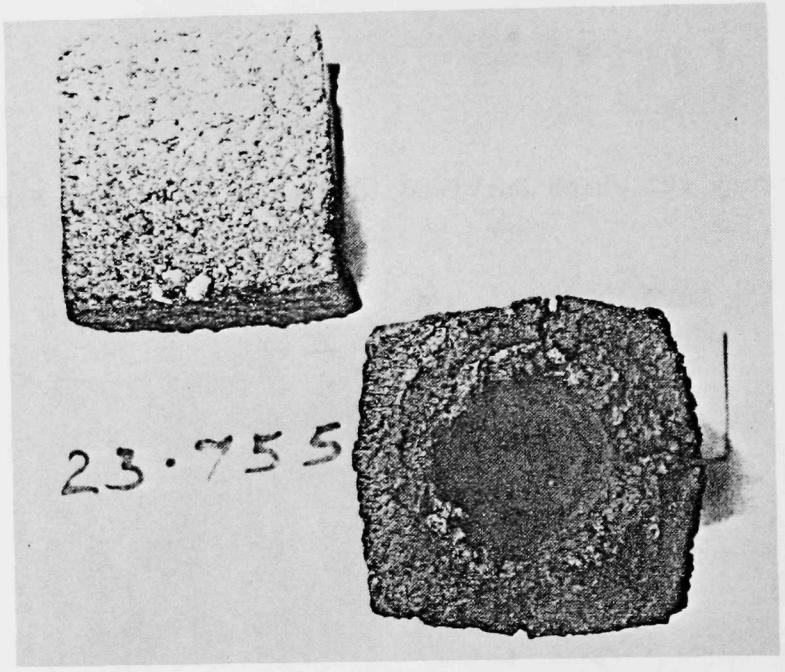

Fig. 3. Refractory #23 which Survived 755 h of Basic Slag Exposure. (Notice microcracks at top surface of cup specimen.)

TABLE V. Grain-bond System of the Refractories*

Refractory Identification No.		Grain-bond System	No. of Hours Survived+	Remarks
2	(B)	Fused Al_2O_3-Fused	1000	Contains 0.4% of alkaline glass
4	(B)	Fused Al_2O_3-Fused (glassy)	>1000	Only 0.03% of alkaline phase
12	(B)	Tab. Al_2O_3-Mullite	750	
16	(B)	Tab. Al_2O_3-Chromia(SS)**	750	
17	(B)	Tab. Al_2O_3-Mullite	750	
18	(CA)	Chrome·Al_2O_3-Phosphate	>1000	Ramming mix
19	(B)	Magnesia·Chrome-Chromia(SS)**	>1000	
20	(B)	Magnesite·Chrome-Solid Solution	>1000	
21	(B)	Magnesite·Chrome-Chromia(SS)**	>1000	
22	(B)	Chrome-Fused	>1000	
23	(B)	Alumina·Chrome-Chromia(SS)**	>1000	

*Survived 750 h or more exposure to basic slag.

**Chromia-alumina solid solution.

+In basic slag.

TABLE VI. Quantitative Results from the Cup Slag-corrosion Test (using Basic Slag)

Refractory Identification No.	Hours Exposed at ~1445°C	Avg. % Wt. Change in Cup Plus Lid	Avg. % Dimensional Change in Cup		Remarks
			Top	Bottom	
2 (B)	4.5	1.1	0	0	Data acquired between 0 and 4.5 h.
	25	2.1	1.5	0	Data acquired between 0 and 25 h.
	238	2.2	5.9	1.6	Data acquired between 0 and 238 h.
4 (B)	100	NA	0	0	No apparent dimensional change or growth.
	1559	NA	0	0	
12 (B)	100	NA	2	0	
	785	NA	35	8	Data acquired between 0 and 785 h.
16 (B)	4.5	3.2	6.2	0	Data acquired between 0 and 4.5 h.
	770	NA	22	4	Cracked at the center of the cup. (Data acquired between 0 and 770 h.)
18 (CA)	1552	-1.5 (loss)	0	0	Data acquired between 1314 and 1552 h. (Matrix was observed to be gradually crumbling.)
19 (B)	1310	NA	<-1	<-1	Appears to be slightly etched or evaporated. (Data acquired between 0 and 1310 h.)
20 (B)	4.5	2.2	0	0	
	1310	NA	<-1	<-1	Appears to be slightly etched or evaporated.
21 (B)	747	2	0	0	Data acquired between 500 and 747 h only.
	1004	2.8	0	0	Data acquired between 747 and 1000 h only.
22 (B)	100	NA	0	0	Very slight dimensional changes between 747 and 1004 h but overall average change is close to 0.
	747	NA	0	0	
	1004	NA	0	0	
23 (B)	498	2	12	0	Data acquired between 260 and 498 h only.
	755	1.9	19	1.5	Data acquired between 498 and 755 h only. (Developed cracks during 498 and 755 h exposure.)
36 (B)	4.5	-1.3	-3.1	0	Data acquired between 0 and 4.5 h.*
	238	-2.8	-4.9	-1.6	Data acquired between 0 and 238 h.*
	495	-5.6	-8.1	-3	Data acquired between 238 and 495 h only.*

*Appears to be glazed with glossy product and evaporated.

The observed data are given in Table VII. Only one refractory (#8) developed cracks and refractories 18, 19, and 21 indicated slight swelling after 100-h exposure. The acidic slag indicated tendency of sticking with refractories 2, 4, and 22 and formed a sandwiched-type weld joint between cup and lid. A similar effect using basic slag was also observed, especially for refractories 2, 4, and 22.

Table VIII gives the quantitative data for weight and dimensional changes before and after exposure. The quantitative dimensional change data are in good agreement with that observed and given in Table VII. Not much meaning could be given to change in weight data as yet(from only two exposures). A meaningful trend may be observed once the 1000-h exposure(s) data are available.

Figures 4, 5, and 6 show the photographs of exposed specimens of refractories #8, 22, and 23, respectively. Figure 4 shows the small cracks which have developed at the interface of slag and refractory. Figure 5 shows the broken two halves of refractory #22 which were produced while separating the slag-welded lid from the cup. Refractory 23, as indicated in Fig. 6, showed negligible or no reaction with slag. It should be noticed that this specimen did not indicate any channel or crack from visual inspection (see Table VII); however, a cut or bottom channel, was observed (see Fig. 6). This may not be the typical of this refractory. Either the channel existed originally or an acidic slag reaction through the pores ($\sim$10%) might have produced a channel. However, the latter is quite unlikely as similar observations were not made in other specimens (of refractory #23) using basic or acidic slags. The data for 1000-h acidic slag is being collected and will be reported in the next quarterly report.

(3) The microstructural analyses of exposed specimens is being carried out to determine the causes of failure of the refractories. The specimens which have been exposed to slag are being analyzed on the basis of generic system, i.e., grain-bond system. The analysis for specimens exposed to basic slag is in progress [illegible]c systems are reported below.

TABLE VII. Cup Slag-corrosion Tests (with Acidic Slag)*

Refractory Identification No.*	Specimen Condition After	
	4.5 h	100 h
2 (B)	P, St	P, St
4 (B)	P, St	P, St
8 (CA)	P, C(S), S	P, C
11 (B)	P	P
12 (B)	P	P
16 (B)	P	P
18 (CA)	P	P, S(S)
19 (B)	P	P, S(S)
20 (B)	P	P
21 (B)	P	P, S(S)
22 (B)	P, St	P, St
23 (B)	P	P
24 (B)	NA	P
25 (B)	NA	NA
36 (B)	P	P

*: At approximately 1545°C.

P: Visible penetration or chemical attack.

C: Visible cracks.

(S): Slight or small.

S: Swollen.

St: Slag sticks to refractory (sometimes slag overflow welds the lid to cup).

(B): Brick or preshaped.

(CA): Castable.

NA: Not available.

TABLE VIII. Quantitative Results from the Cup Slag-corrosion Test (using Acidic Slag)*

Refractory Identification No.		Range of Exposed Hours	Avg. % Wt. Change in Cup Plus Lid	Avg. % Dimensional Change in Cup	
				Top	Bottom
2	(B)	0-4.5	1.5	0	0
		0-100	<1	0	0
4	(B)	0-4.5	1.3	0	0
		0-100	<1	0	0
8	(CA)	0-4.5	2.1	1.5	<1
		0-100	4.7	1.4	<1
11	(B)	0-4.5	4	0	0
		0-100	-2	1.4	0
12	(B)	0-4.5	1.7	0	0
		0-100	1.8	3.7	<1
16	(B)	0-4.5	3.1	0	0
		0-100	2.6	1.4	0
18	(CA)	0-4.5	-1	1.6	0
		0-100	-5.8	6.1	1.5
19	(B)	0-4.5	2.1	0	0
		0-100	4.2	3.0	2.2
20	(B)	0-4.5	3.7	0	0
		0-100	NA	NA	NA
21	(B)	0-4.5	2.9	1.5	<1
		0-100	6.8	3.7	3.1
22	(B)	0-4.5	2.2	0	0
		0-100	-1.3	0	0
23	(B)	0-4.5	2.7	0	0
		0-100	3.8	1.4	0
24	(B)	0-4.5	NA	NA	NA
		0-100	<1	1.5	<1
36	(B)	0-4.5	<1	1.5	0
		0-100	NA	2.1	0

*: At approximately 1545°C

NA: Not available.

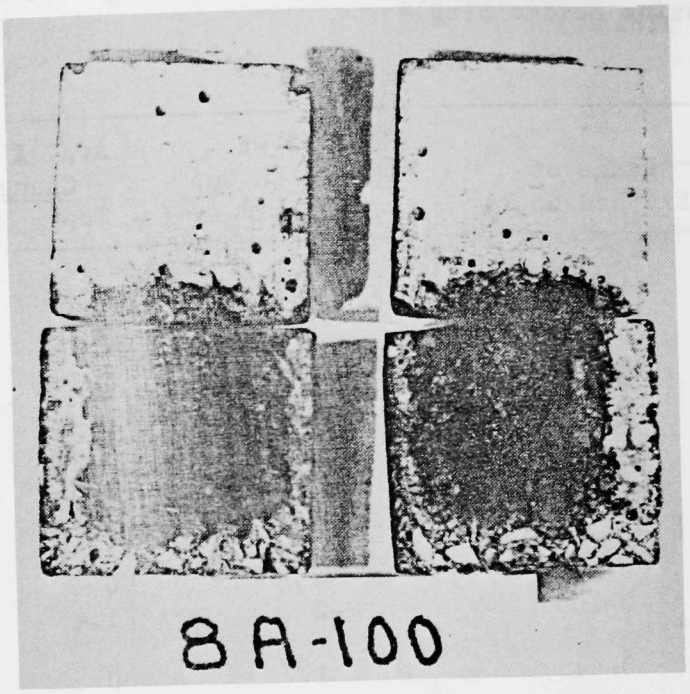

Fig. 4. Refractory #8 after 100-h Exposure to Acidic Slag. (Observe deterioration of internal surface with some microcracks.)

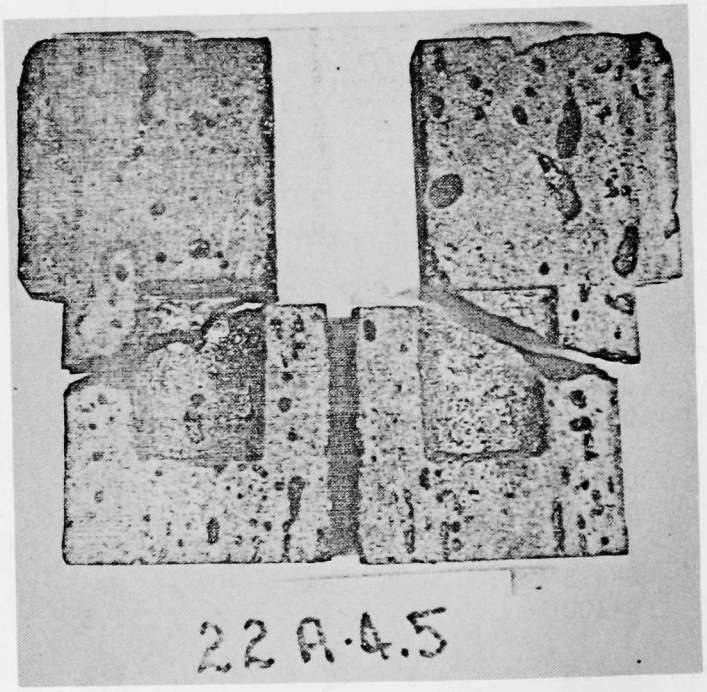

Fig. 5. Refractory #22 after 4.5-h Exposure to Acidic Slag. (Notice the cup was cracked during separating slag-welded lid to the cup.)

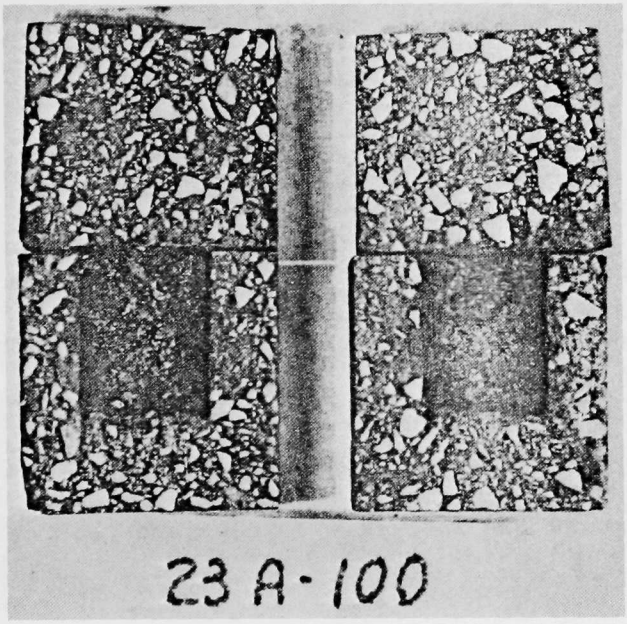

Fig. 6. Refractory #23 after 100-h Exposure to Acidic Slag.

(i) Tabular alumina grain - sintered bond (with minute clay product): This system is typical of refractories #1 and 3. When a refractory of this system is exposed to basic slag, two types of reactions appear to take place between the refractory and basic slag. These are:

$$6Al_2O_3 \text{ (grain)} + CaO \text{ (slag)} \longrightarrow CaO \cdot 6Al_2O_3 \ (CA_6) \quad (1)$$

$$2Al_2O_3 \text{ (grain)} + XCaO \cdot YSiO_2 \cdot ZNa_2O \text{ (slag)} \longrightarrow CaO \cdot Al_2O_3 \cdot SiO_2 + Na_2O \cdot Al_2O_3 \cdot 2SiO_2 \ (NAS_2) \quad (2)$$

The first reaction, which is a predominant one, forms calcium hexaluminate needles (see Fig. 7) and these needles grow with time, i.e., the reaction is time dependent. Simultaneously, reaction (2) proceeds at a slow rate and forms glassy product ($CaO \cdot Al_2O_3 \cdot SiO_2$) and a small quantity of nepheline ($Na_2O \cdot Al_2O_3 \cdot 2SiO_2$) around the needles of CA_6. Figure 7 shows the microstructural changes in the refractory as a result of the two above-mentioned reactions. The cause of failure, i.e., development of cracks and swelling with time, is attributed to the formation of CA_6 which has molar volume seven times that of alumina. Thus, the formation of CA_6 expands the lattice with time and this causes the swelling, etc.

(ii) Tabular alumina grain-mullite bond: This system is typical of refractories #11, 12, 13, 14, and 15. Refractories 11 and 12 contained a small amount of phosphate bond (this is not indicated in Table I for refractory 12).* The reactions which take place between refractory and basic slag are as follows:

$$Al_2O_3 \text{ (grain)} + XCaO \cdot YSiO_2 \text{ (slag)} \longrightarrow CaO \cdot Al_2O_3 \cdot 2SiO_2 \ (CAS_2) \quad (3)$$
(anorthite)

$$Al_2O_3 \cdot 2SiO_2 \text{ (mullite bond)} + XCaO \cdot YSiO_2 \cdot ZAl_2O_3 \text{ (slag)} \longrightarrow \longrightarrow CAS_2 + \alpha\text{-}Al_2O_3 \text{ (recrystallized)} \quad (4)$$

*Private communication between ANL and supplier.

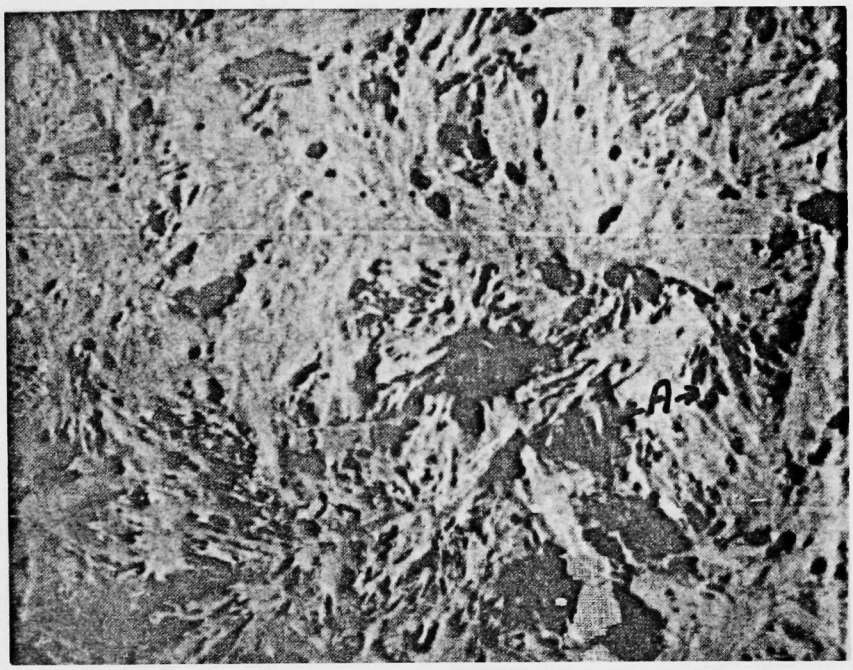

Fig. 7. Microstructure of Reacted Zone from Refractory #1 after 505-h Basic-Slag Exposure. Calcium hexaluminate needles (A); surrounded by complex phases of slag silicates ($CaO \cdot Al_2O_3 \cdot SiO_2$).

$$XAl_2O_3 \cdot YSiO_2 \cdot ZP_2O_5 \text{ (bond)} + PCaO \cdot QAl_2O_3 \text{ (slag)} \longrightarrow CAS_2 + \alpha\text{-}Al_2O_3 \text{ (recrystallized)} + \text{(slag silicates·phosphates)} \quad (5)$$

$$Al_2O_3 \text{ (tab. or secondary)} + XMgO \cdot YFe_2O_3 \text{ (slag)} \longrightarrow (Mg \cdot Fe)O \cdot (Al \cdot Fe)_2O_3 \text{(spinel)} + \text{slag silicates} \quad (6)$$

The failure of this type of refractory appears to take place by the disintegration of the bond as well as the grain. Reaction (3) indicates the reaction between grain and slag and thus forming anorthite (CAS_2). The mullite bond reacts with slag and forms anorthite and secondary recrystallized alumina, as indicated by reaction (4). The tabular alumina as well as secondary alumina react with slag to form a complex spinel of the type indicated by reaction (6). In the case of the phosphate bond (refractories 11 and 12), slag disintegrates the bond (see reaction 5) and forms complex anorthite and α-Al_2O_3 which are surrounded by a complex phase of slag silicates and phosphates. Figure 8 shows the microstructural features of tabular Al_2O_3-mullite type refractory after exposure to basic slag for 785 h. The figure is self-explanatory with respect to the above-mentioned reaction products.

b. Slag-abrasion-corrosion Test Rig

As reported earlier,[1,2] the slag-abrasion-corrosion test rig has been constructed to determine the resistance of refractories to the simultaneous abrasive and corrosive attack by slag in simulated environments.

The hookup of utilities (except for oxygen) was completed on Sept. 30, 1975. The safety test runs for water, air, and gas were conducted. All the systems with interlocks operated as expected. However, a safety point was raised by the ANL Safety Committee. Since the environment of the chamber will be changed to CO/CO_2 from H_2O/O_2, i.e., reducing rather than oxidizing, there should be an interlock system between air and gas to automatically shut the gas if air (or O_2)

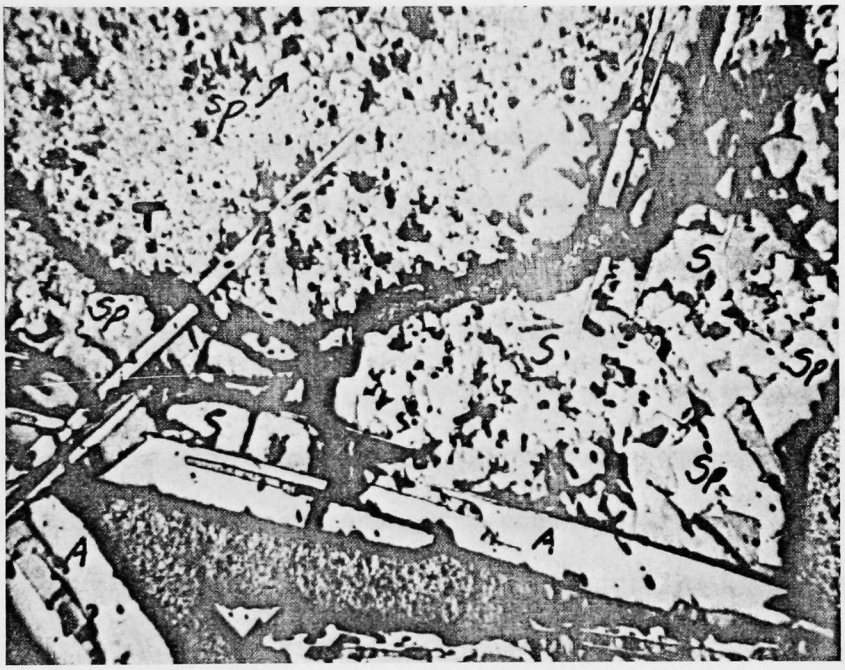

Fig. 8. A Typical Microstructure of Reacted Refractory #12. This belongs to a specimen exposed to basic slag for 785 h. T: tabular alumina; A: recrystallized alumina; Sp: $(Mg \cdot Fe)O \cdot (Al \cdot Fe)_2O_3$ (spinel); S: anorthite.

supply fails (or exhausts) during a long-time run. The present system could release a high-temperature combustible product into the exhaust duct through room air. To avoid this problem, four separate air-gas interlock systems will be installed for each burner. This work is in progress and hopefully should be finished by the end of October 1975. The oxygen solenoid valve for the oxygen line has not been received yet but they are expected to be received by the end of October 1975. The first run is planned by the end of December 1975.

c. Future Work

The future effort in this program will be as follows:

(1) The failed and unfailed refractory specimens exposed to basic and acidic slag will be analyzed microscopically to determine the failure mechanisms and to identify newly formed phases or product(s). This is a continuing effort between ANL and the suppliers.

(2) The 1000-h exposure of refractories to acidic slag will be completed.

(3) The preliminary test runs using the slag-abrasion-corrosion rig will be conducted on selected refractories.

Task B -- Evaluation of Ceramic Coatings for Coal-conversion Plants
(Principal Investigator: R. Swaroop)

The ceramic coating program has progressed in the following areas during the past four months: (a) the preparation of coatings using plasma spray and other techniques; (b) the study of thermal spalling in various substrate-coating systems as a result of thermal shock; (c) the exposure of coated specimens to a coal-gas mixture; and (d) the construction of a one atmosphere erosion-corrosion apparatus (in cooperation with Task 4).

a. Preparation of Coatings

(1) Plasma spray coatings (≈250 μm thick) of Al_2O_3, $Al_2O_3 \cdot MgO$, ZrO_2, $MgO \cdot ZrO_2$, and Cr_3C_2 were prepared over substrates of Types 304, 310, and 316 stainless steel (SS). Various intermediate layers of metal and/or alloys were tried to reduce the spalling effect during thermal cycling (980 → 50°C). The intermediate layers included pure aluminum, nickel, chromium, an alloy of nickel-chromium, and an alloy of nickel-chromium-aluminum. The experiments were conducted in a stepwise manner so that the thermal-cycling resistance of each intermediate layer could be determined. The results of this study are reported in Section (b). The hardnesses of some of the as-produced coatings are given in Table IX.

(2) Boron-diffused (boride) coatings (≈50 μm) on Type 304SS and IN800 were produced using Lindeberg's Boroloy process. This process involves gaseous diffusion accompanied by pack-cementation. The process was carried out for up to 4 h at 1850°F (2100°C) Thermal-cycling and corrosion tests on these specimens will be carried out in the next three months.

(3) Ion-plated coatings of Al_2O_3 and Al-Al_2O_3 and Hf-Al_2O_3 were produced on Type 304SS. The ceramic coatings (aluminum oxide) were between 20 and 100 μm thick with metal-intermediate layer of 1 to 3 μm thick. Figure 9 shows the micrograph of Hf-Al_2O_3 coating on Type 304SS. The adherence and tenacity of the coating to the substrate was excellent. The corrosion and thermal-cycling resistance of these specimens will be reported in subsequent sections.

TABLE IX. Hardness of Plasma Sprayed Coatings on Type 304SS

Coating	Hardness (R_c)
Al_2O_3	63-69
Al_2O_3 (50% Cr_2O_3)	60-65
ZrO_2 (CaO-stabilized)	55-62
MgO Al_2O_3 (spinel)	60-65
MgO ZrO_2 (24:76)	45-50
Cr_3C_2 (45%) + (Ni-Al)	64-68

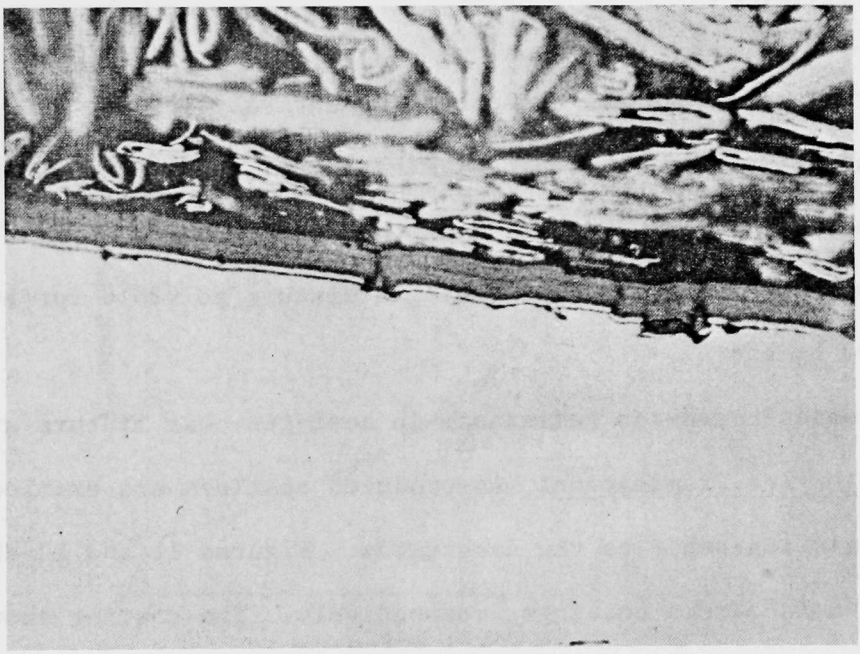

Fig. 9. Ion-plated Hf-Al_2O_3 on Type 304 SS. Mag. 500X.

The ion plating rate of Al_2O_3 was investigated with argon partial pressure in the chamber. It was observed that rate increased with increase in argon partial pressure and Figure 10 indicates the observed effect. Aluminum oxide ion plating rates up to 12 μm/min were observed at 20 microns of argon partial pressure.

Further development work is required to ion plate thicker oxide, mixed oxides and spinel with an intermediate layer to reduce the thermal-expansion mismatch between the substrate and ceramic coating.

b. Evaluation

The ceramic coatings are evaluated sequentially for:

(1) Integrity by microscopic examination of substrate-coating interface;

(2) Thermal-cycling (-shock) resistance;

(3) Corrosion resistance in coal-gas mixture at 980°C for 100 and 500 h; and

(4) Erosion-corrosion resistance in coal-gas-char mixture at 980°C.

(1) Interface Examination: As-produced coatings are examined microscopically for their adherence to the substrates. Figures 11 and 12 show examples of adherent and nonadherent coatings, respectively. The coating shown in Fig. 11 was produced by an ion-plating method while that shown in Fig. 12 was produced via plasma spray technique. Figure 13 shows a micrograph of an adherent plasma-sprayed coating with an intermediate bond coat. The coatings which have an intermediate channel (see Fig. 12) would not survive the thermal-shock test and hence, would fail in the first evaluation test. The plasma-spray technique has generally produced adherent coatings if specified deposition parameters were followed for spraying. The ion-plating method has so far produced ceramic coatings of excellent adherence, tenacity, and density.

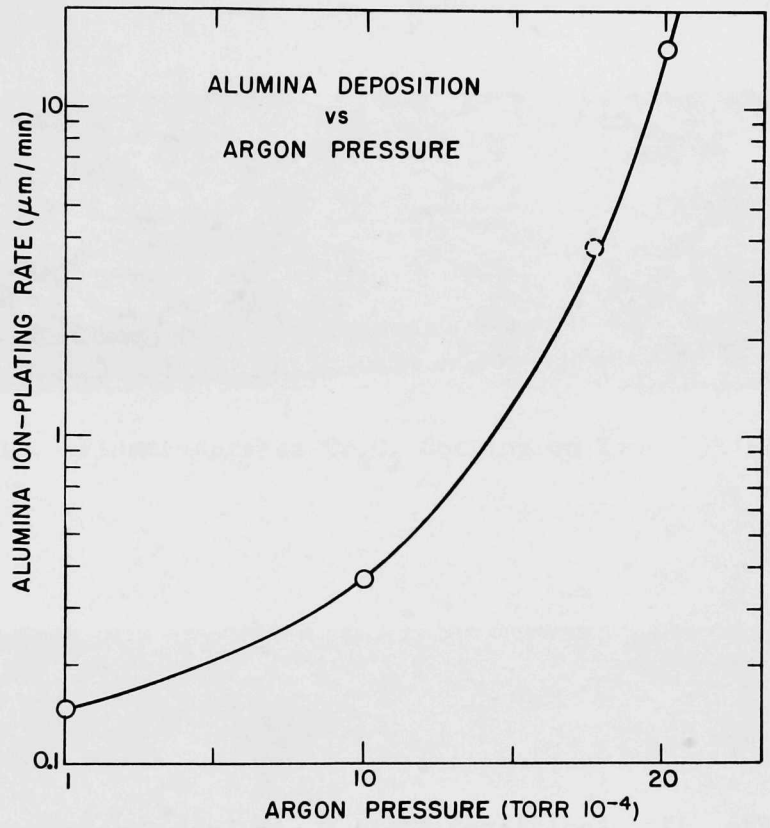

Fig. 10. Ion-plating Rate Dependence on Partial Pressure of Argon.

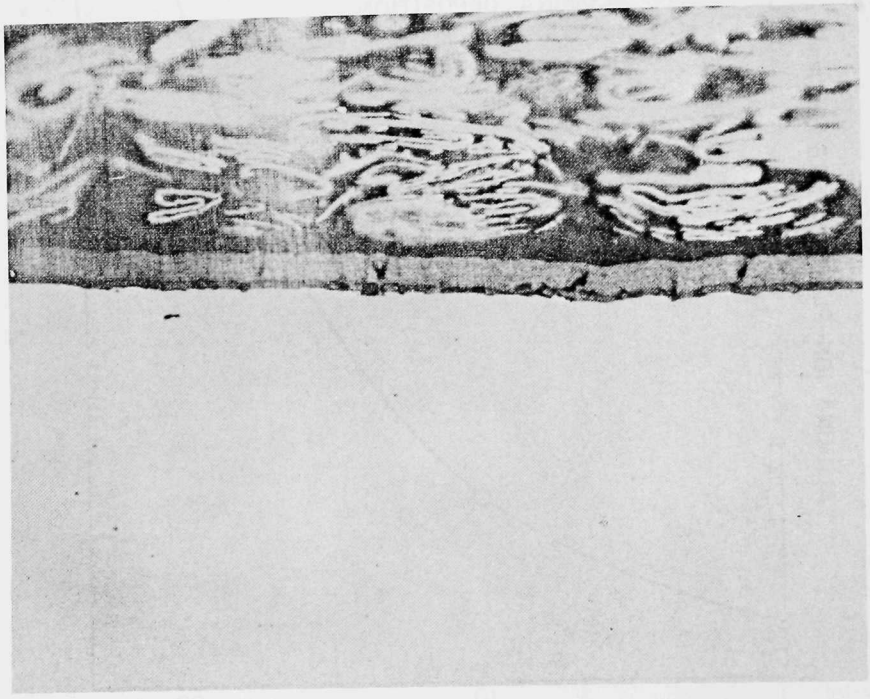

Fig. 11. Ion-plated Al-Al_2O_3 on Type 304 SS. Mag. 500X.

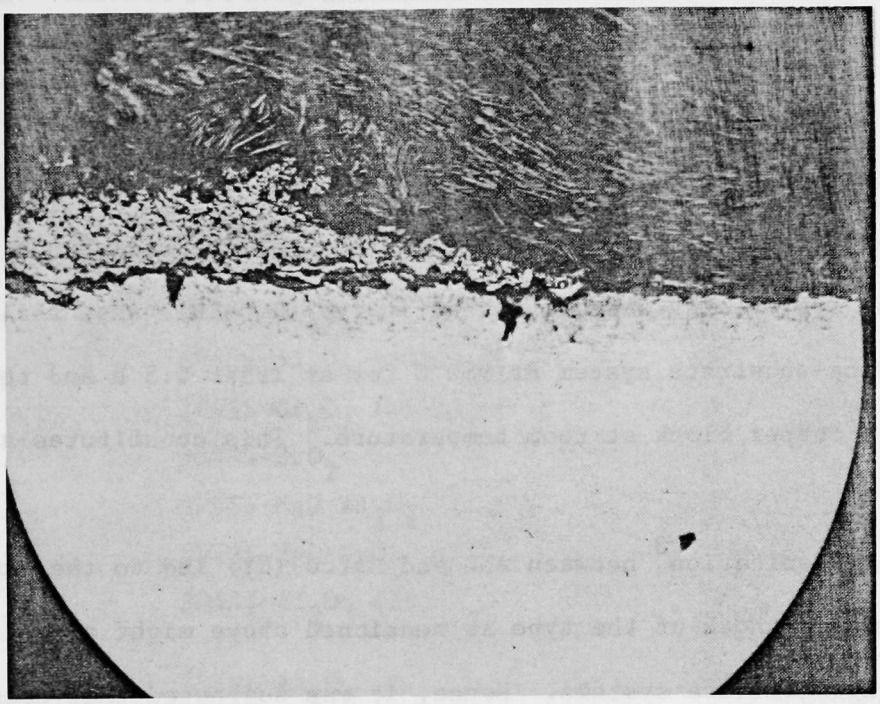

Fig. 12. Plasma-sprayed Cr_3C_2 Coating on Type 304 SS.

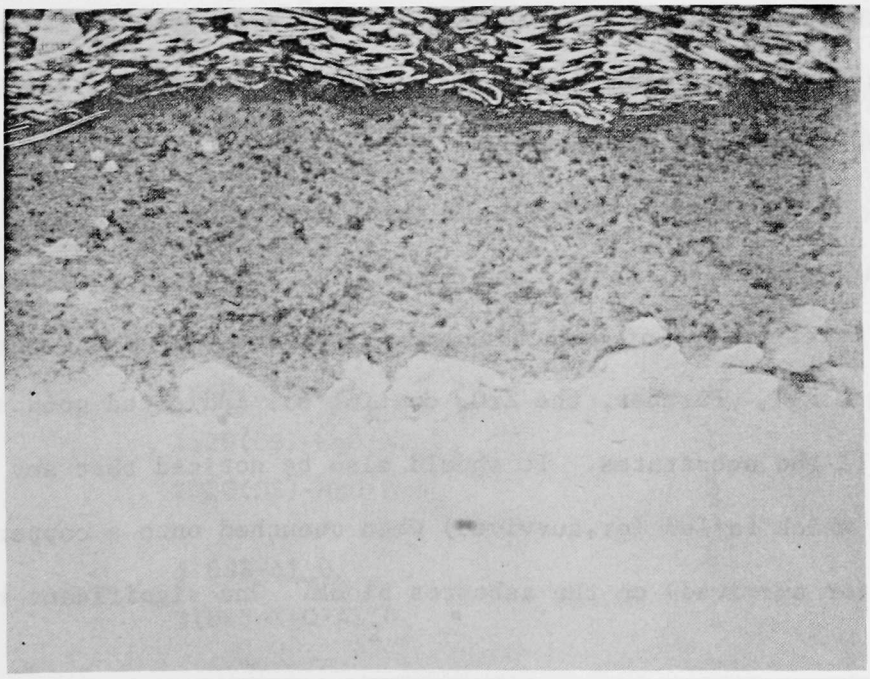

Fig. 13. Plasma-sprayed Al_2O_3 with (Ni-Cr-Al) Bond Coat. Mag. 200X.

(2) Thermal-shock (-cycling) Experiments: As explained in the third quarterly report,[2] spalling of coatings during heating or cooling is a problem, which, in turn, affects the corrosion resistance of the coatings. This effect is due to mismatch between thermal expansion coefficients of the coating and substrate. An experiment to roughly determine the spalling resistance of various substrate-coating systems has been explained in ref. 2. This essentially involves soaking the coating-substrate system at 980°C for at least 0.5 h and then quenching the system onto a copper block at room temperature. This constitutes a single thermal cycle.

A communication[3] between ANL and Metco (NY) led to the warning that a severe thermal shock of the type as mentioned above might exclude many reasonable coating-substrate systems. Hence, it was suggested that specimens should be quenched onto an asbestos block (or sheet) rather than onto a copper block. This modification would then sort out relatively weak systems to which an intermediate bond-coat approach could be attempted. A retesting of the various coating-substrate systems was then conducted. Table X gives the results of a number of cycles that each system has passed before spalling as a result of quenching the system on asbestos or copper blocks.

It is apparent from Table IX that coatings Al_2O_3, Al_2O_3 + (50% Cr_2O_3), and $MgO \cdot Al_2O_3$ on Types 304SS, 316SS, and IN800 have indicated spalling during thermal-cycling irrespective of quenching rate (asbestos-quenching rate is slower than copper-quenching). Further, the ZrO_2 coating has indicated good spalling resistance for all the substrates. It should also be noticed that any coating-substrate system which failed (or survived) when quenched onto a copper block has also failed (or survived) on the asbestos block. One significant result

TABLE X. Thermal-cycling Test for Various Substrate-coating Systems

Specimen Identification No.	Substrate-coating System	No. of Cycles (Before Spalling)	
		Asbestos Chilled	Copper Chilled
A9	304SS-Al_2O_3	1	1
A10	304SS-Al_2O_3 (50%Cr_2O_3)	1	1
A11	304SS-Cr_3C_2 (Ni-Al)	4^+	4^+
A12	304SS-ZrO_2	4^+	NA
A13	304SS-$MgO \cdot Al_2O_3$	1	1
A14	304SS-$MgO \cdot ZrO_2$	NA	NA
A60	304SS-Al_2O_3 (IP)	4^+	1
B9	316SS-Al_2O_3	1	1
B10	316SS-Al_2O_3 (50%Cr_2O_3)	1	1
B13	316SS-$MgO \cdot Al_2O_3$	1	1
C9	IN800-Al_2O_3	1	1
C10	IN800-Al_2O_3 (50%Cr_2O_3)	NA	1
C11	IN800-Cr_3C_2 (Ni-Al)	4^+	4^+
C12	IN800-ZrO_2	4^+	4^+
C13	IN800-$MgO \cdot Al_2O_3$	1	1
C14	IN800-$MgO \cdot ZrO_2$	4^+	4^+
D9	1020(CS)-Al_2O_3	2	NA
D10	1020(CS)-Al_2O_3 (50%Cr_2O_3)	1	NA
D11	1020(CS)-Cr_3C_2 (Ni-Al)	4^+	4^+
D12	1020(CS)-ZrO_2	4^+	4^+
D13	1020(CS)-$MgO \cdot Al_2O_3$	1	1
D14	1020(CS)-$MgO \cdot ZrO_2$	2	NA
E9	310SS-Al_2O_3	1	1
E13	310SS-$MgO \cdot Al_2O_3$	1	1

$^+$: Terminated.

NA: Not available.

obtained from these data is that a coating of chromium carbide blended with Ni-Al alloy (#11) survived the thermal-cycling tests irrespective of the substrate. This clearly suggests that nickel-rich matrix is producing the bond between substrate and coating. This observation led to the series of experiments mentioned below.

Various intermediate metal and alloy layers were tried between the ceramic coating and substrate. These were aluminum, chromium, nickel-chromium, and nickel-chromium-aluminum. The diffused layer of aluminum or chromium did not improve the spalling resistance while nickel-chromium (50-50 alloy) or nickel-chromium-aluminum (75-24-1) alloy indicated a remarkably improved spalling resistance. Table XI gives the results obtained from a plasma-sprayed Al_2O_3 coating on Type 304 SS. The thicknesses of the intermediate layer were between 50 and 70 μm while that of the ceramic coating was between 200 and 250 μm.

The data given in Table X indicate that the nickel-rich intermediate layer with a chromium content around 25% should be able to improve the spalling resistance of ceramic coatings. The commercially available alloy of nickel-chromium-aluminum (75-24-1) was therefore selected to be used as an intermediate bond between substrate and coating. It should be mentioned that high chromium content (>25%) in the bond coat (intermediate layer) may reduce the spalling resistance at high temperature because of the brittle nature of high-chromium alloys.[4]

A number of coatings with an intermediate layer of (Ni-Cr-Al) alloy were prepared on various substrates. Table XII gives the results of thermal-shock tests obtained from these systems (substrate/bond coat/coating). It is evident from this table that thermal spalling resistance has been improved remarkably such that some of the coatings did not even show a sign of thermal-

TABLE XI. Effect of Bond Coat on Thermal Spalling

Substrate	Intermediate Layer (≈60 μm)	Coating (≈200 μm)	No. of Cycles	Remarks
304SS	Al	Al_2O_3	1	S
304SS	Chromium	Al_2O_3	1	S
304SS	Ni-Cr (50/50)	Al_2O_3	2-3	S
304SS	Ni-Cr-Al (75-24-1)	Al_2O_3	5^+	G

$^+$: Terminated. S: Spalled. G: Did not spall.

TABLE XII. Thermal Shock Resistance of Coatings* (with Bond Coat)$^+$

Substrate-Coating	No. of Cycles** (980-50)°C	Specimen Identification No.
304-BC-Al_2O_3	3^{++}	A9T
316-BC-Al_2O_3	5^{++}	B9T
310-BC-Al_2O_3	5^{++}	E9T
IN800-BC-Al_2O_3	5^{++}	C9T

*: 200-250 μm.
**: Survived before spalling.
$^+$: 60-80 μm thick.
$^{++}$: Terminated (without spalling).
BC: Ni-Cr-Al (75-24-1).

cracking up to 5 thermal cycles. Figure 14 shows the various coating-substrate systems which have survived up to 5 thermal cycles or more (for identification of samples, see Table X).

The Al_2O_3 coatings which were produced via the ion plating method have indicated excellent thermal-spalling resistance when a thin (2-3 μm) intermediate layer of either Al or Hf was ion plated between the substrate and coating. Table XIII gives the results of thermal-cycling tests conducted on such coating-substrate systems. The Al_2O_3 coatings were between 26 and 100 μm. Figure 15 shows the ion plated Al_2O_3 coating which survived several thermal cycles.

(3) Corrosion Testing of Ceramic Coatings: Various coated substrates were evaluated in a representative coal-gas mixture such as that produced in one of the high-BTU pilot plants. The average composition of the coal-gas mixture used in these tests is given in Table XIV. The experiments were conducted at 980°C for 100 and 500 h at 1 atm. pressure. The gas mixture was flowing through the retort at a rate that would produce an exchange of one retort volume every 10 min.

The quick criteria for the ability of a coating to resist corrosion and protect the substrate is determined by examining the exposed specimen under 10 to 50X magnification. Figure 16 explains these criteria. If the coating has resisted (R) or retarded (R,M) the corrosion, the platinum wire wound around the specimen appears at the top of coating, otherwise it is buried underneath the corrosion product. The specimens which have shown to be resistant to gaseous corrosion are then analyzed for micro-reaction zone boundaries and reaction products (if any) using the optical microscope and SEM.

During the last four months approximately 20 coating-substrate systems were evaluated (in three runs) in a coal-gas mixture of 980°C. Table XV lists the tested coating-substrate systems along with the observed results.

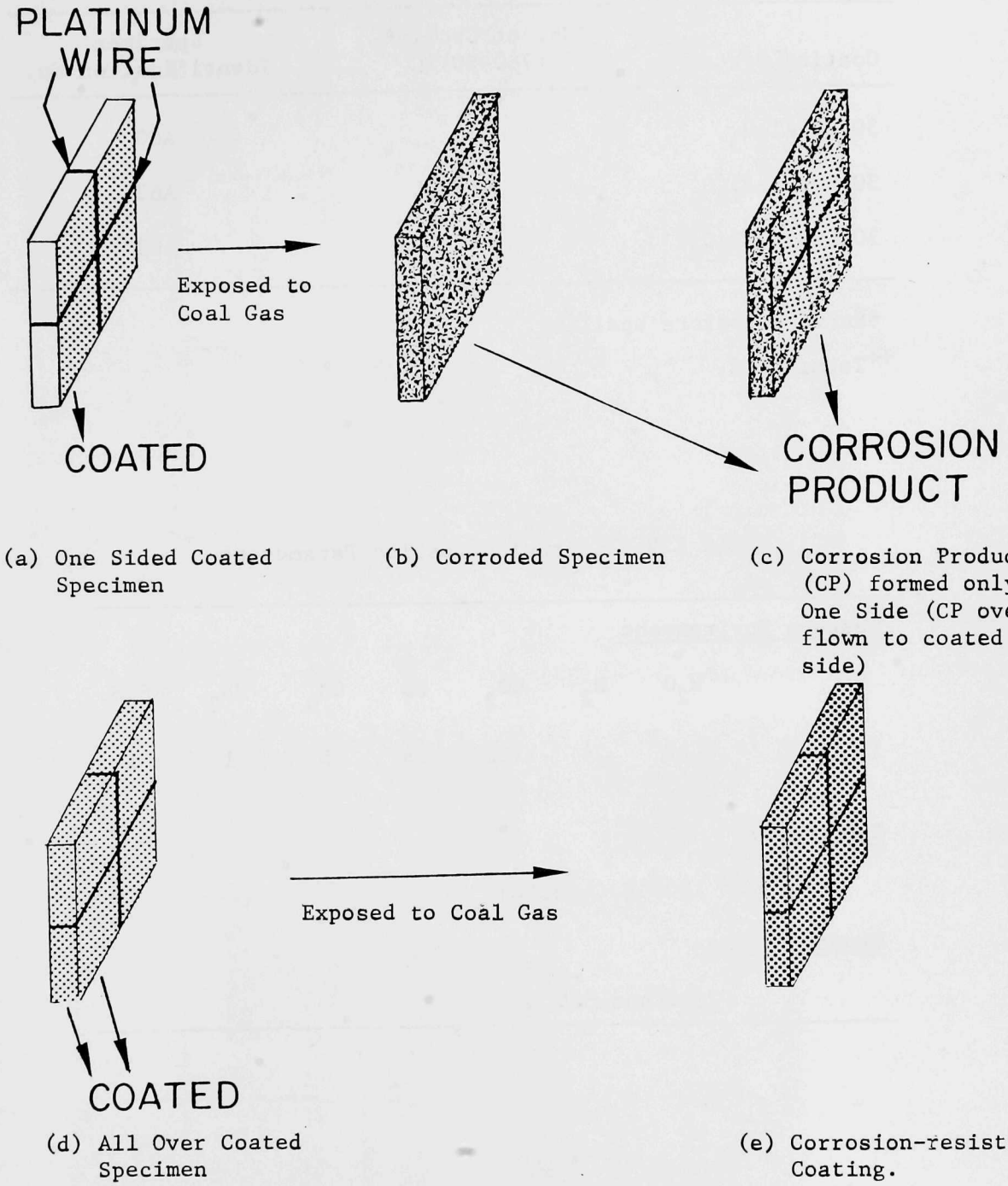

Fig. 14. Schematic of Corrosion Testing of Coated Specimen.

TABLE XIII. Thermal-shock Resistance of Ion-plated Coatings

Coating System	No. of Cycles* (980-50)°C	Specimen Identification No.
304SS-Al_2O_3	1	A60
304SS-Al-Al_2O_3	4++	A62
304SS-Hf-Al_2O_3	4++	A63

*Survived before spalling.

++Terminated.

TABLE XIV. Corrosion Testing Parameters

Gaseous Environment

	H_2O	H_2	CO_2	CO	CH_4	NH_3	H_2S
(Vol. %)	39	24	12	18	5	1	1

Temperature

1800°F (∿980°C)

Exposure Time

100 and 500 h

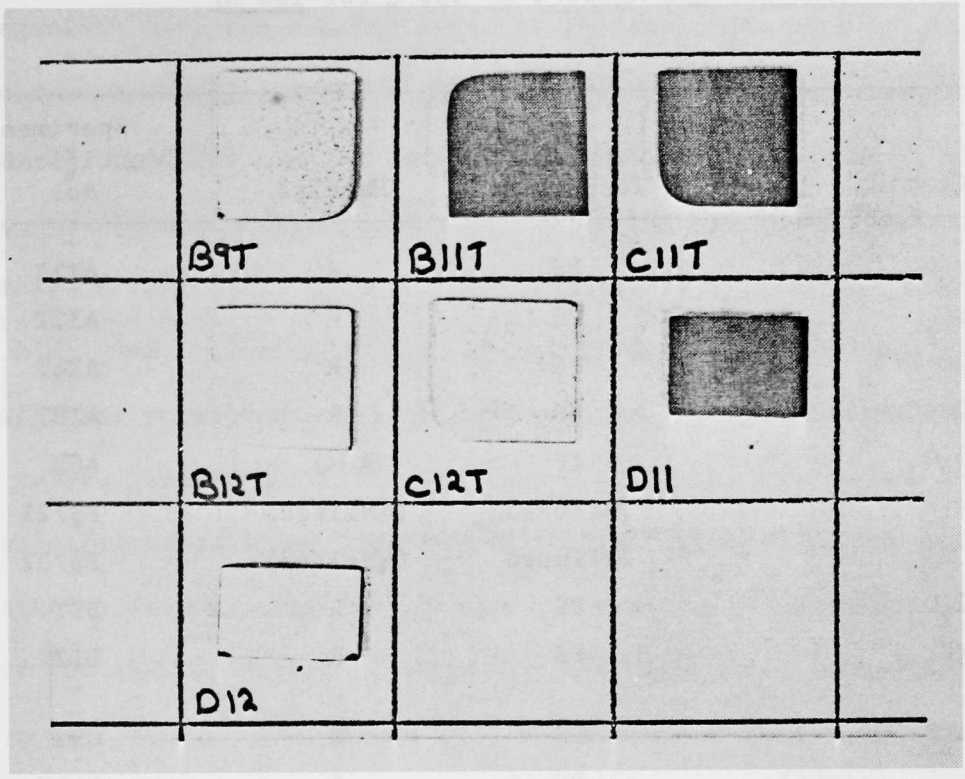

Fig. 15. Coating-substrate Systems* which Survived Five Thermal Cycles (or more). *For identification, see Table X.

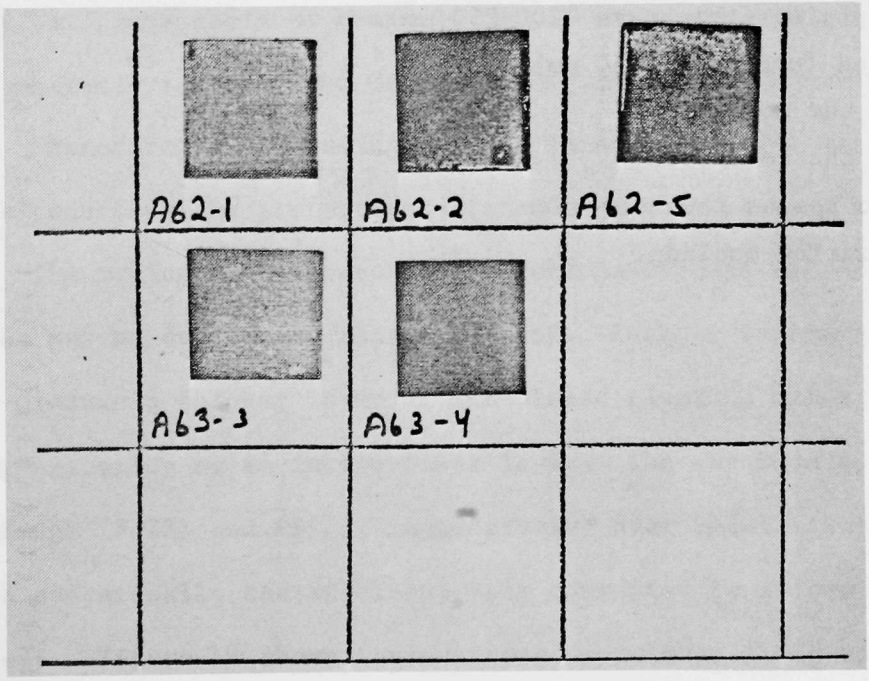

Fig. 16. Ion-plated Hf-Al_2O_3 and Al-Al_2O_3 on Type 304 SS; these Survived Several Thermal Cycles.

TABLE XV. Corrosion Testing of Various Coating-substrate Systems (In Coal-gas Mixture at 980°C for 100 h)

Substrate Coating	Deposition Technique	Results	Specimen Identification No.
304SS-BC-Cr_3C_2 (Ni-Al)	PS	R	A11T
304SS-BC-ZrO_2	PS	R	A12T
304SS-BC-$MgO \cdot ZrO_2$	PS	R	A14T
304SS-BC-(Co-Cr-Al) Alloy	PS	R	A18T
304SS-Hf-Al_2O_3	IP	R(M)	A63
SA285-Cr	Diffused	C(Melted)	FS721
SA285-Cr + Al	Diffused	C(Melted)	FS732
316SS-BC-Al_2O_3	PS	R	B9T
316SS-BC-ZrO_2	PS	R	B12T
IN800-BC-Al_2O_3	PS	R	C9T
IN800-BC-Cr_3C_2 (Ni-Al)	PS	R	C11T
IN800-BC-ZrO_2	PS	R	C12T

PS: Plasma sprayed (thickness ≈200-250 μm).

IP: Ion plated (thickness ≈30 μm).

R: Resisted the corrosion.

R(M): Retarded the corrosion.

C: Failed to resist the corrosion.

S: Spalled during cooling.

The protection performance of the coatings may be divided into three categories: (i) the coating protects the substrate with or without minor spalling and/or corrosion at the edges, (ii) the protection of the substrate by the coating is of medium quality because of spalling or degradation of the coating with time, and (iii) the protection offered by the coating is poor and thus the substrate is corroded. These three categories are listed in Tables XV and XVI as R, R(M), and C, respectively. It should be emphasized that the main objectives of these experiments are to find suitable ceramic coatings which can resist or retard gaseous corrosion and thus protect the substrate. Therefore, coatings categorized as R and R(M) have the potential of offering extended service life in actual practice. Figures 17a and 17b show the specimen exposed to coal-gas mixture for 100 h. Figure 18 shows the specimens which were exposed to coal-gas mixture for 500 h. From Table XVI, it is obvious that coatings Al_2O_3, ZrO_2, and $MgO \cdot ZrO_2$ have survived exposure up to 500 h. The bond coat of (Ni-Cr-Al) alloy was used for some of the coating-substrate systems. All the coatings except Cr_3C_2 (B8 and C11) have resisted corrosion by the coal-gas mixture. As reported in the last quarterly report,[2] the Cr_3C_2 coating had provided corrosion resistance up to 100 h. Therefore, this coating appears to have degraded with time (between 100 and 500 h) and thus the protection offered by such a coating will be limited.

The medium grade corrosion resistance offered by ion-plated aluminum oxide may be due to too thin a coating. Further experiments are being conducted to produce a thicker layer of ion-plated aluminum oxide with ion-plated (Ni-Cr-Al) alloy as an intermediate layer. The chromium and aluminum-chromium coatings (FS721 and FS723, respectively) over SA285 alloy did not resist the corrosion and actually the specimens were converted to molten sulfide eutectic during the test. Figure 19 shows these exposed specimens along with one as-coated specimen. Because of these results, the SA285 substrates diffused with chromium

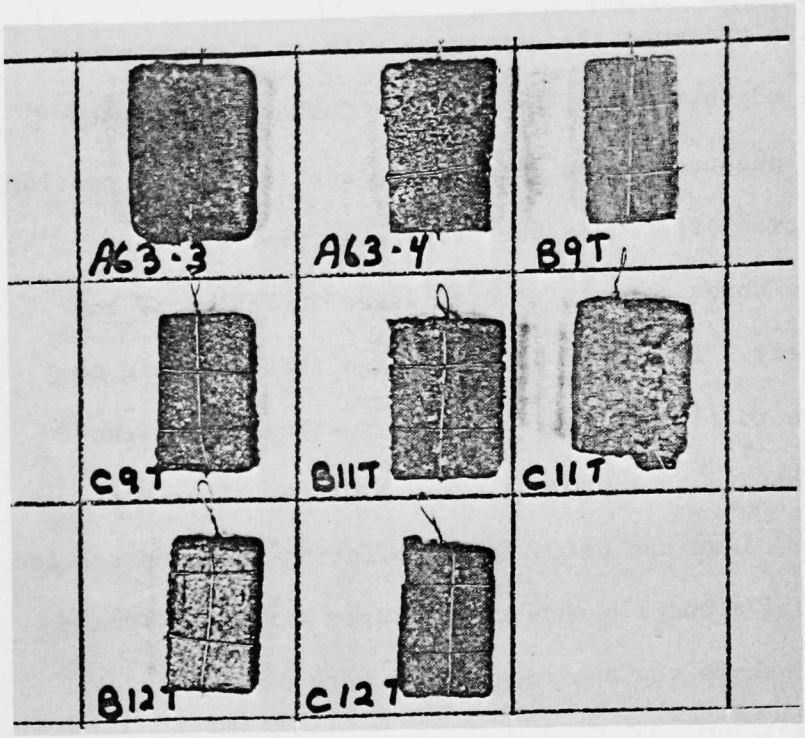

(a) Various Coatings. For identification, see Table X.

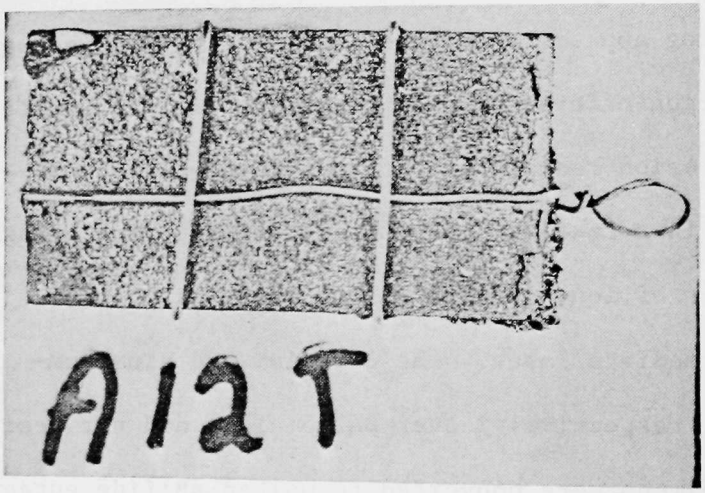

(b) ZrO_2 Coating on Type 304 SS with Bond Coat.

Fig. 17. Coatings after Exposed to Coal-gas Mixture for 100 h.

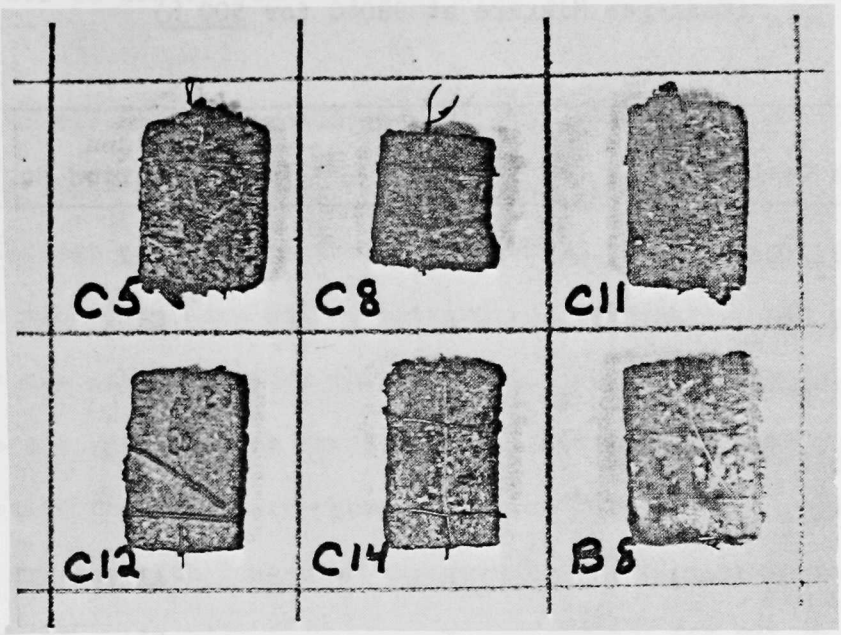

Fig. 18. Various Coating-substrate Systems after 500-h Exposure to Coal-gas Mixture.

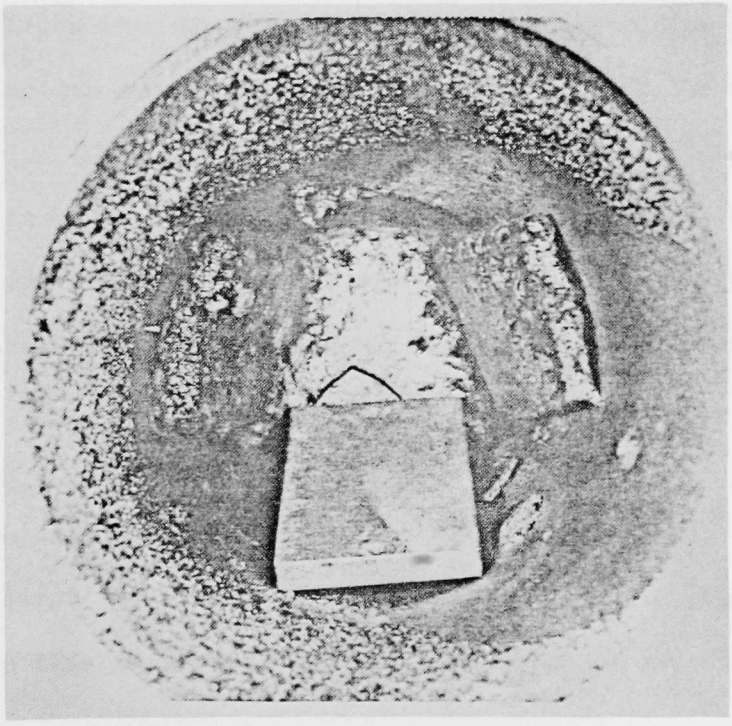

Fig. 19. Chromium- and Aluminum-diffused SA285 Alloy after 100-h Exposure in Coal-gas Mixture; Bottom Specimen is Diffused.

TABLE XVI. Corrosion Testing of Plasma Sprayed Coatings*
(Coal-gas Mixture at 980°C for 500 h)

Substrate Coating	Results	Specimen Identification No.
IN800-ZrO_2 (CaO)	R	C12
IN800-MgO ZrO_2	R	C14
316SS-Cr_3C_2 (25% Ni-Cr)	C	B8
IN800-Cr_3C_2 (25% Ni-Cr)	R(M)	C8
316SS-BC-Al_2O_3	R,S	B9T
304SS-BC-ZrO_2 (CaO)	R	A12T
IN800-Cr_2C_2 (Ni-Al)	C	C11

*: 200-250 μm. R: Resisted; R(M): Retarded corrosion.
C: Corroded. S: Slight spalling during cooling.

and aluminum will be coated with Al_2O_3 or ZrO_2 coatings and evaluated by the corrosion test.

An extensive microscopic analysis of exposed specimens is in progress, using light microscopic, SEM and X-ray techniques. The micrographs of selected coatings are being shown in Figures 20 through 24. The details given for each micrograph are self explanatory. The conclusions are: (i) Al_2O_3 oxide protects the substrate from the gaseous corrosion provided the coating is dense and does not spall during exposure, (ii) chromium carbide (Ni-Cr matrix) appears to protect the substrate above 100 h but not for 500 h. However, this coating disintegrates with long-time exposure to coal-gas mixture (at 980°C) and thus offers no protection from gaseous corrosion.

c. Erosion-corrosion Test Apparatus

As reported earlier,[2] this apparatus is being constructed to evaluate the ceramic-coated and refractory specimens for simultaneous erosion-corrosion resistance in coal-gas-char mixture at 980°C. This apparatus is designed for evaluating one specimen at one atmospheric pressure under the conditions of erosive wear.

All the required materials for this apparatus have been received and parts are being constructed in the ANL machine shop. These are expected to be completed by December 1975. The assembly drawing of this apparatus is shown in Fig. 25.

d. Corrosion-erosion Test at Solar, Inc.

Per conversation between Solar and ANL,[5] Solar should be ready to proceed with the first test run by November 1975. Solar is preparing a first progress report in this work which should be received by ANL shortly.

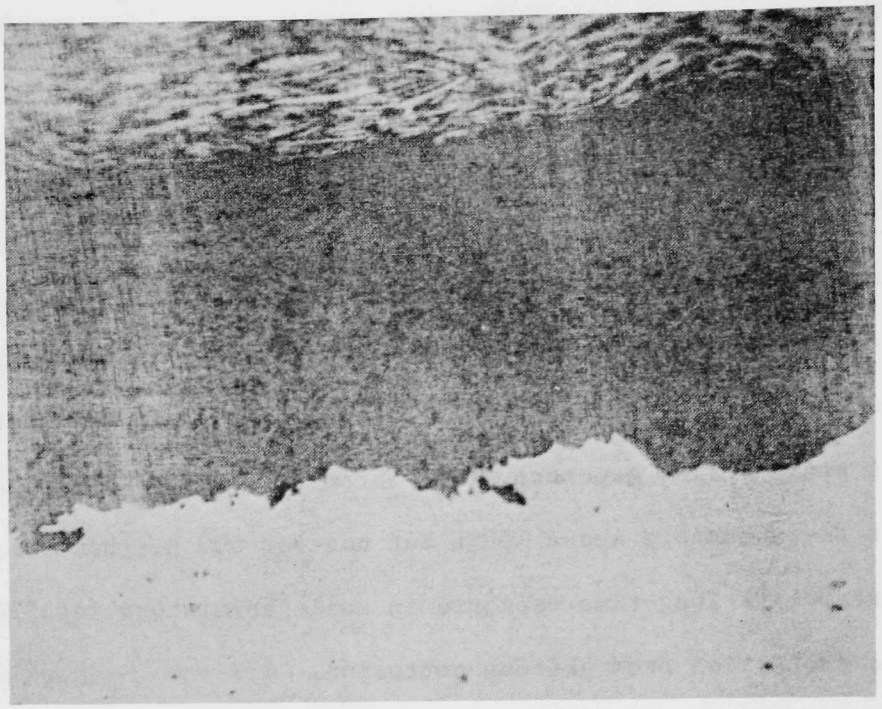

Fig. 20. Plasma-sprayed Al_2O_3 Coating on IN800. Mag. 200X.

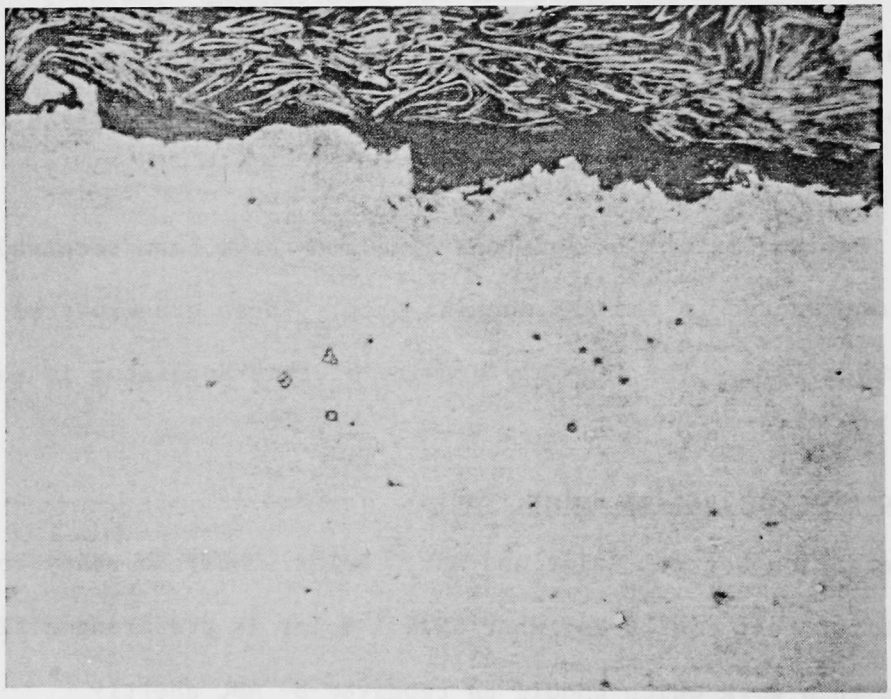

Fig. 21. Coating Shown in Fig. 20 after 100-h Exposure in Coal-gas Mixture. (Note: Coating protected substrate but spalled during cooling.) Mag. 200X.

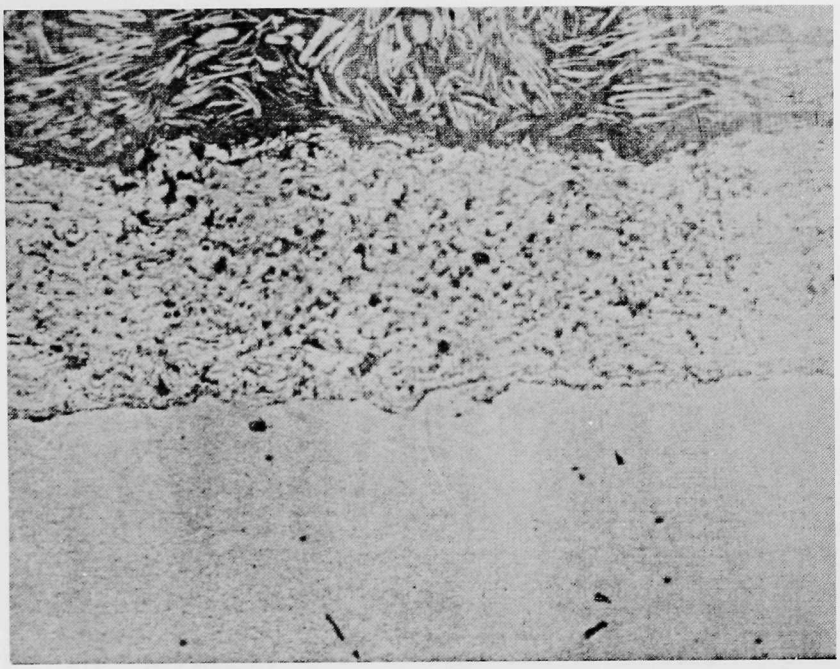

Fig. 22. Plasma-sprayed Cr_3C_2 Coating on IN800. Mag. 200X.

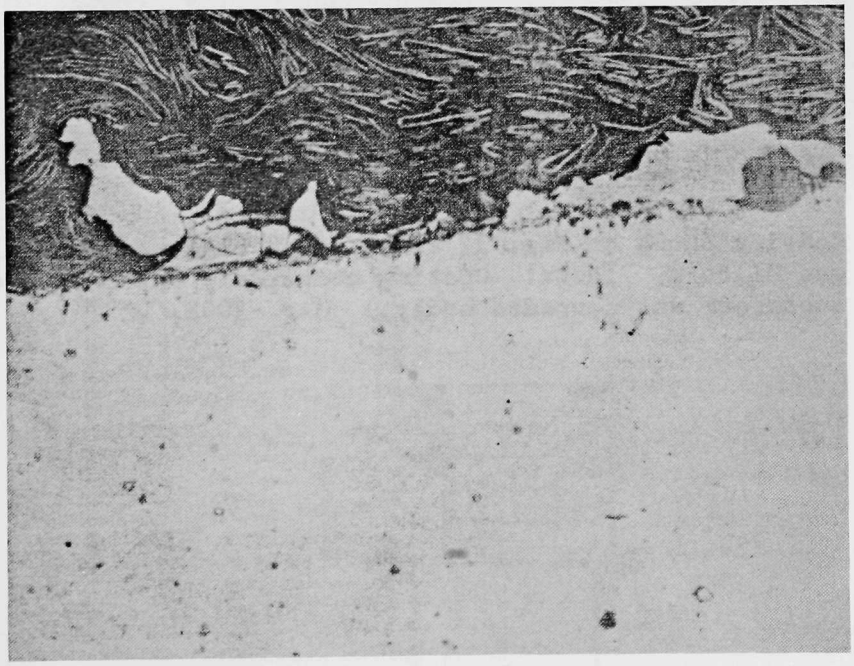

Fig. 23. Coating Shown in Fig. 22 after 100-h Exposure in Coal-gas Mixture. (Note: Coating protected the substrate although consumed or spalled.) Mag. 200X.

Fig. 24. Coating Shown in Fig. 22 after 500-h Exposure in Coal-gas Mixture. (Note: Coating completely consumed and substrate was corroded badly.) Mag. 200X.

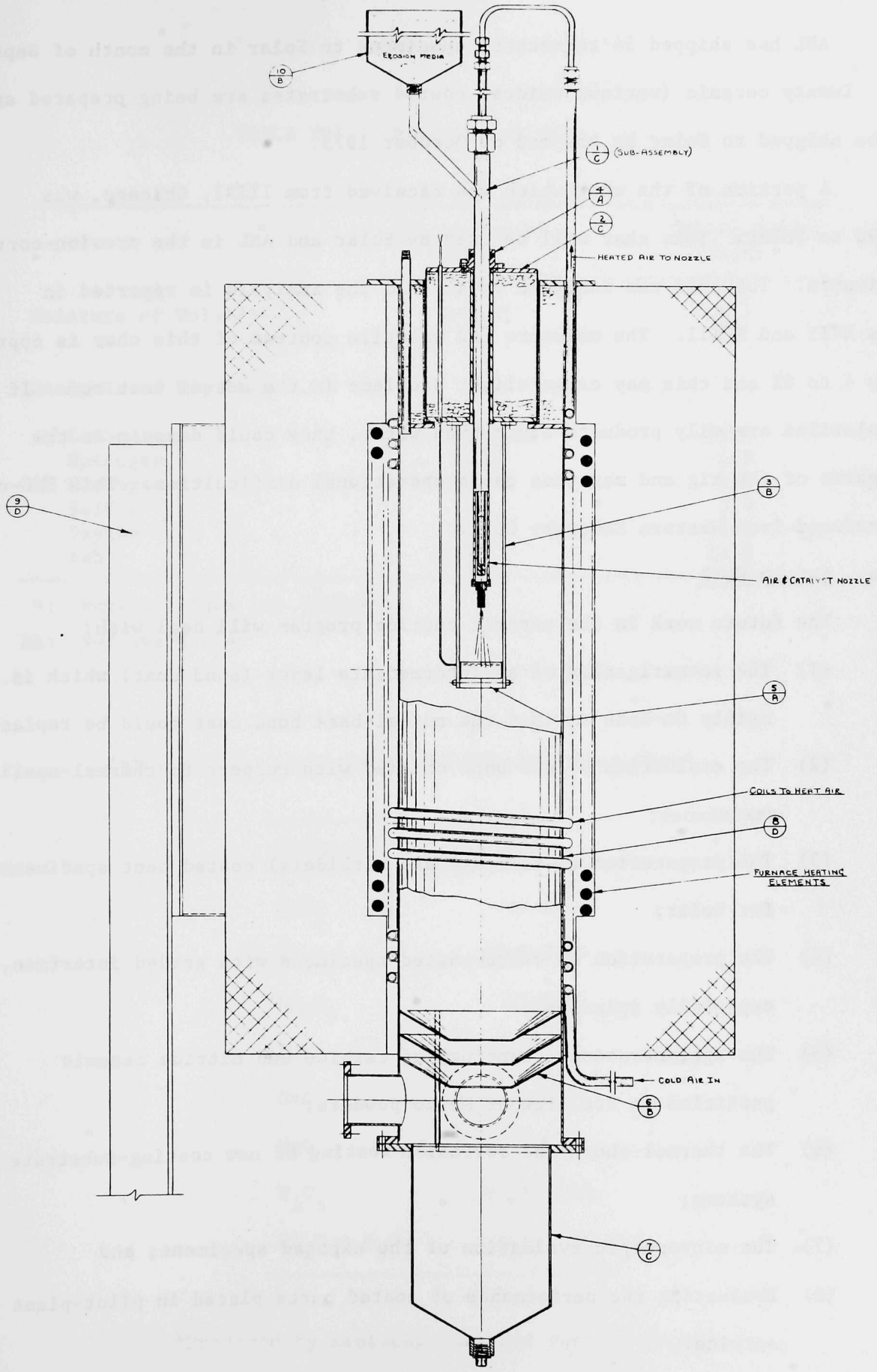

Schematic of Erosion-corrosion Apparatus.

ANL has shipped 54 refractory specimens to Solar in the month of September 1975. Twenty ceramic (various oxides) coated substrates are being prepared and will be shipped to Solar by the end of October 1975.

A portion of the char which was received from IITRI, Chicago, was shipped to Solar. This char will be used by Solar and ANL in the erosion-corrosion experiments. The char was analyzed by ANL and the analysis is reported in Tables XVII and XVIII. The moisture and volatile content of this char is approximately 4 to 6% and this may cause slight problems in the actual test run. If the volatiles are oily products other than water, they could deposit in the cold parts of the rig and may thus cause operational difficulties. This FMC-char was produced from Western Kentucky Coal.

e. Future Work

The future work in the ceramic coating program will deal with:

(1) The investigation of an intermediate layer (bond coat) which is mainly Co-base so that the nickel-base bond coat could be replaced;

(2) The evaluation of new bond coat(s) with respect to thermal-spalling resistance;

(3) The preparation of oxide(s) and carbide(s) coated bent specimens for Solar;

(4) The preparation of oxide-coated specimens with graded interface, especially spinel(s);

(5) The agglomeration (trapping) of carbide and nitride ceramic particles in Stellite or Metco powders;

(6) The thermal-shock and corrosion testing of new coating-substrate systems;

(7) The microscopic evaluation of the exposed specimens; and

(8) Evaluating the performance of coated parts placed in pilot-plant service.

TABLE XVII. Analysis of Char

	ANL Analysis* (wt.%)	FMC Analysis (wt.%)
Moisture of Volatile	4-4.25	6.4
Analysis of Dry Char		
Carbon	76.9-77.3	75.9
Hydrogen	0.91	1.9
Nitrogen	1.9-2.0	1.6
Sulfur	NA	3.0
Oxygen	8.2	3.1
Ash	11-11.7	14.5

*: Reported from two analyses.

NA: Not available.

TABLE XVIII. Analysis of Ash Obtained from Char*

Compound	Wt.%
SiO_2	43-43.5
Al_2O_3	19.6-21.9
Fe_2O_3	25-25.7
SO_3	6.7-7.5
CaO	2.5-2.7
MgO	1.8-1.9
P_2O_5	0.02-0.03
$Na_2O + K_2O$	1.5-3.0

*Produced by Kentucky Coal and sent to Solar.

References

1. ANL Second Quarterly Report to FE/ERDA, March 15, 1975.

2. ANL Third Quarterly Report to FE/ERDA, June 15, 1975.

3. Private communication between Metco and ANL.

4. G. G. Wood, J. G. Wright, T. Hodgkress, and D. P. Whittle, Werkstoffe U. Korrosion 21 900 (1970).

5. Telecons between V. Moore (Solar) and R. Swaroop (ANL) during Sept.-Oct. 1975.

TASK C) Nondestructive Testing for Coal-plant Components (W. A. Ellingson)

1. Infrared

The new AGA Model 750 portable scanning camera system with wide angle and telephoto lenses was received this quarter. After initial checkout tests, a series of calibration curves were obtained. Since some field applications involve viewing through flame sheets, calibration curves were obtained with and without flame filters and through flame sheets. These calibration curves are shown in Figs. 1-4 of this section.

An initial field study was conducted on subsystems of the CO_2 Acceptor Plant in Rapid City. The coal crushing system and coal lift lines were examined for thermal gradients. The coal crushing system is in an enclosed area but the lift lines were open to the atmosphere. An infrared photograph of the coal crushing system is shown in Fig. 5 along with a line drawing indicating the various components. Regions with no insulation are clearly observable as the white regions. Subsequent more sensitive scans were clearly able to establish thermal gradients within the high temperature regions. Immediate future field plans include returning to the CO_2 plant (week of October 20) to examine the heater tubes on the recycle gas heater. Future laboratory plans include investigating refractory crack patterns as a function of several parameters, and expansion joints, and blocked tees for operating and erosion pattern characteristics.

2. Radiography

Two field trips have been made this quarter to the Battelle Agglomerating Ash plant, in West Jefferson, Ohio, for experimental radiographic testing of refractory layered structures. The first trip, July 29-31,

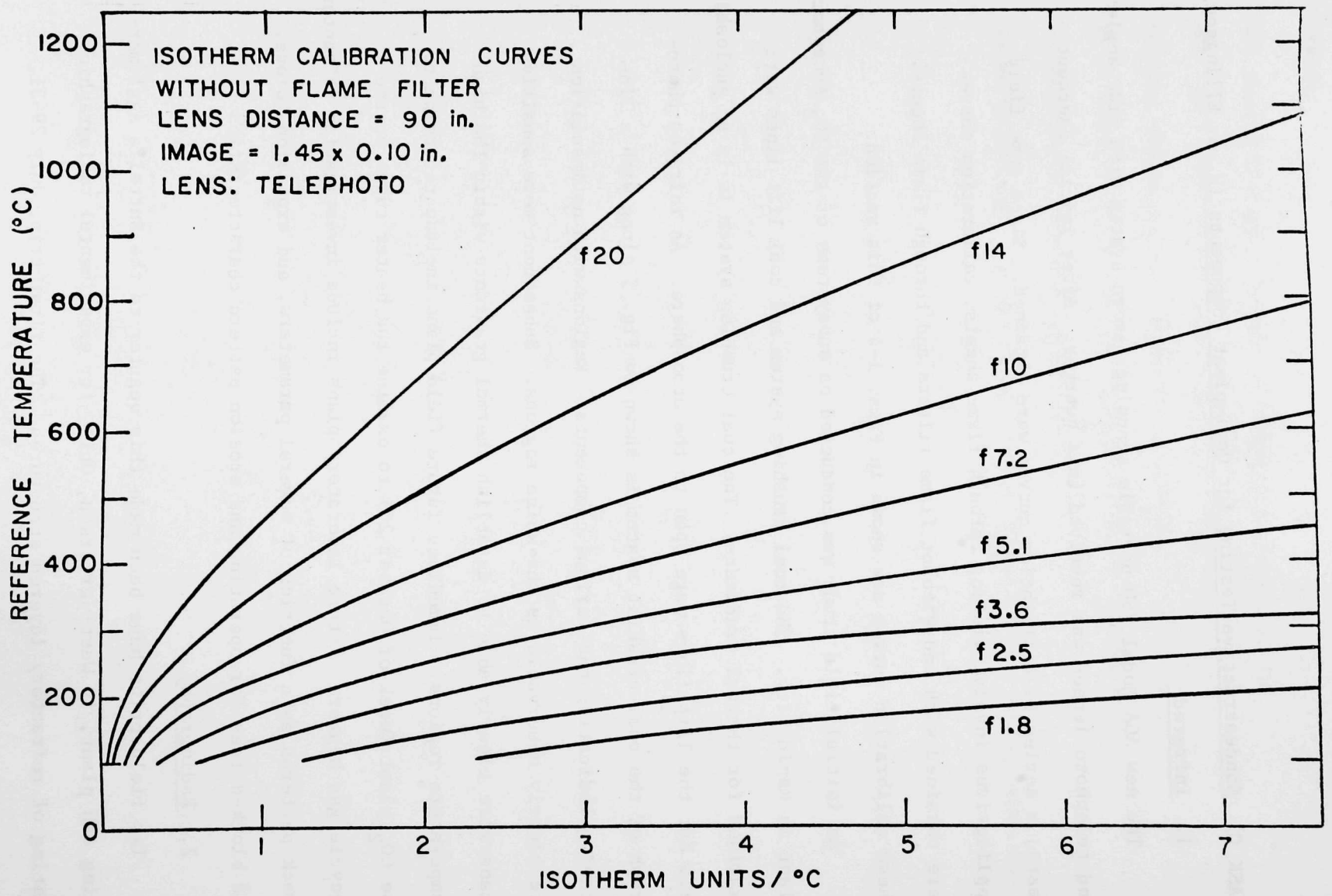

Fig. 1. AGA Model 750 Calibration.

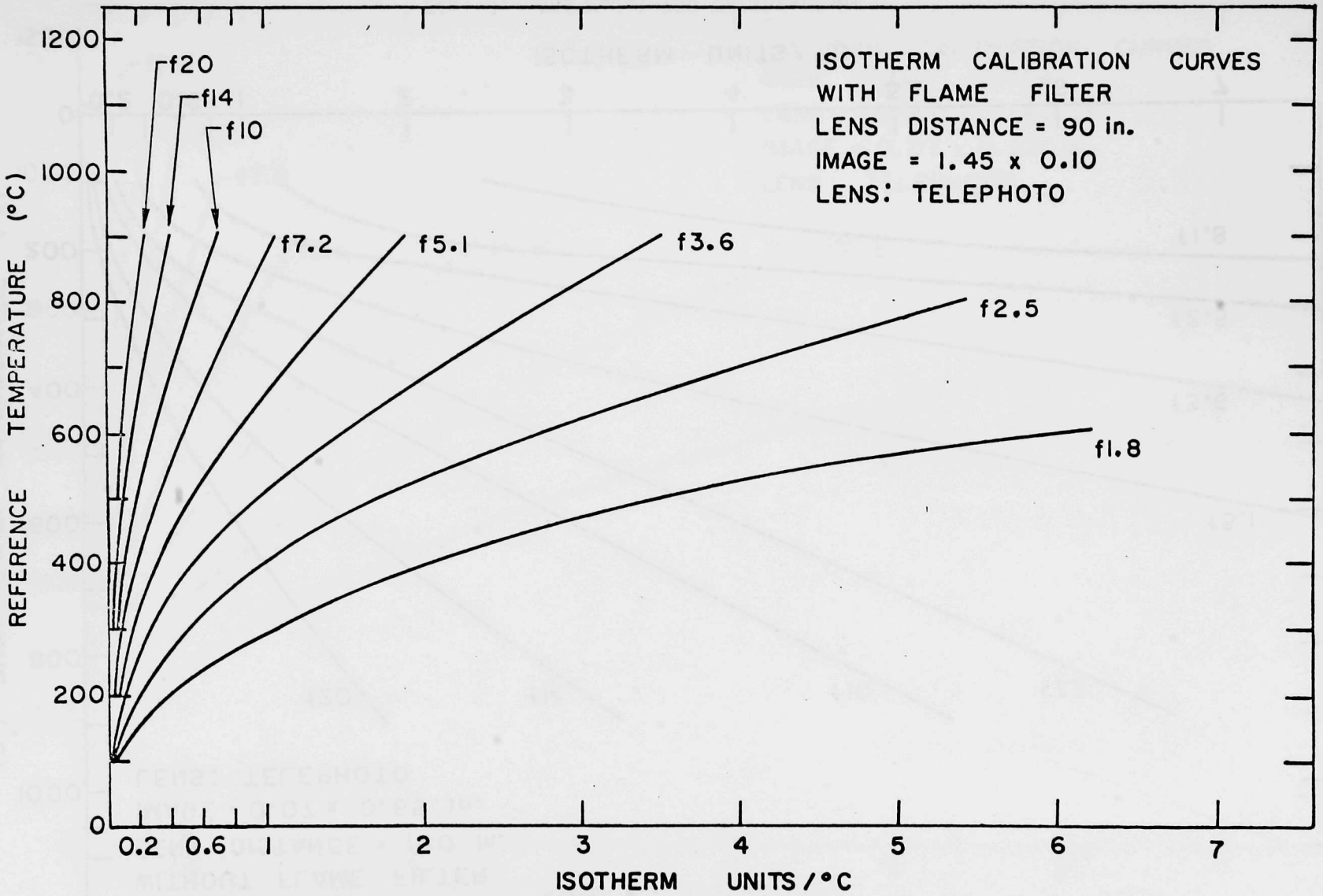

Fig. 2. AGA Model 750 Calibration.

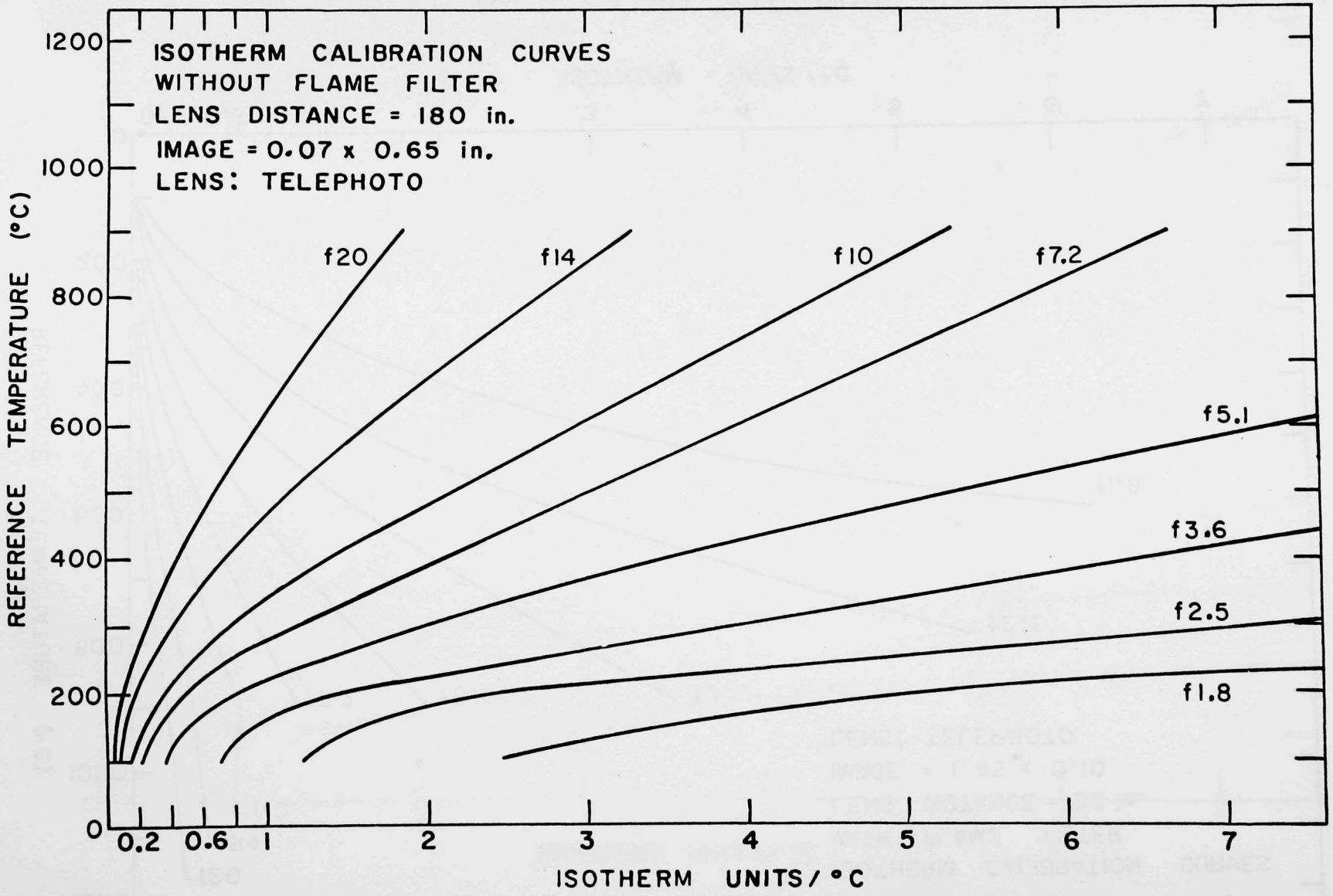

Fig. 3. AGA Model 750 Calibration.

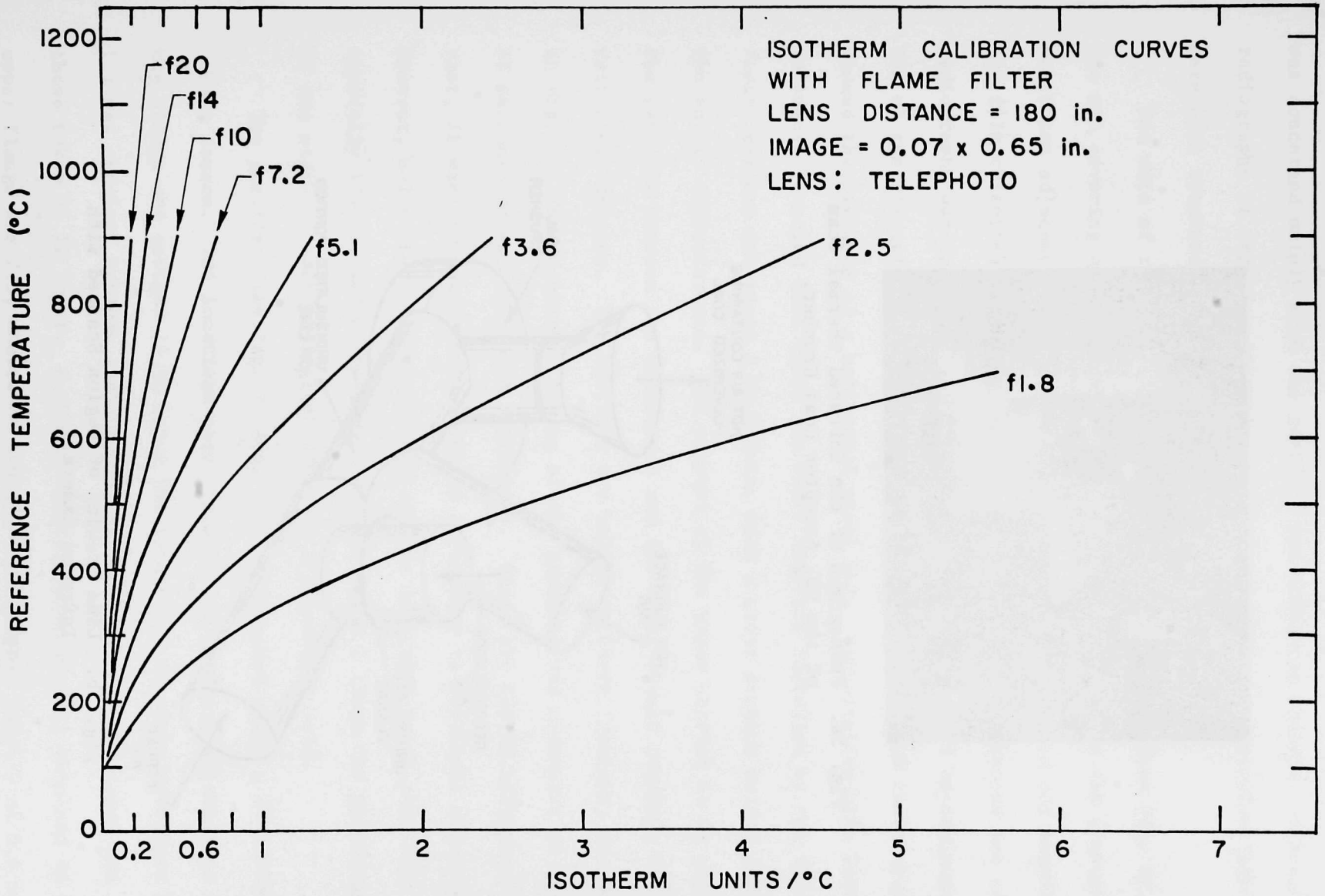

Fig. 4. AGA Model 750 Calibration.

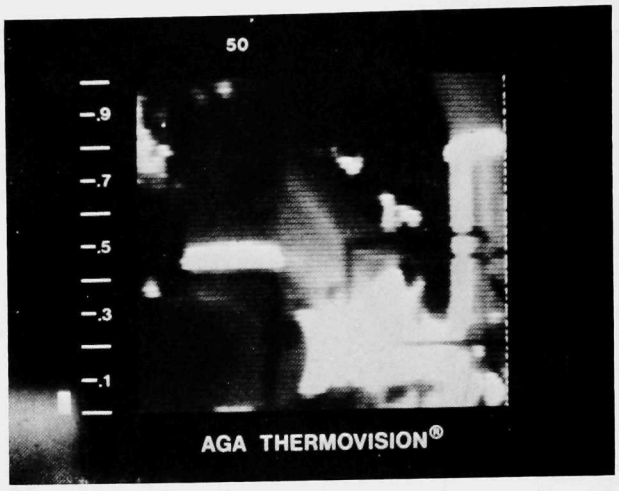

Fig. 5a. Photograph of the infrared thermal Scan of the CO_2 Acceptor Coal Crusher.

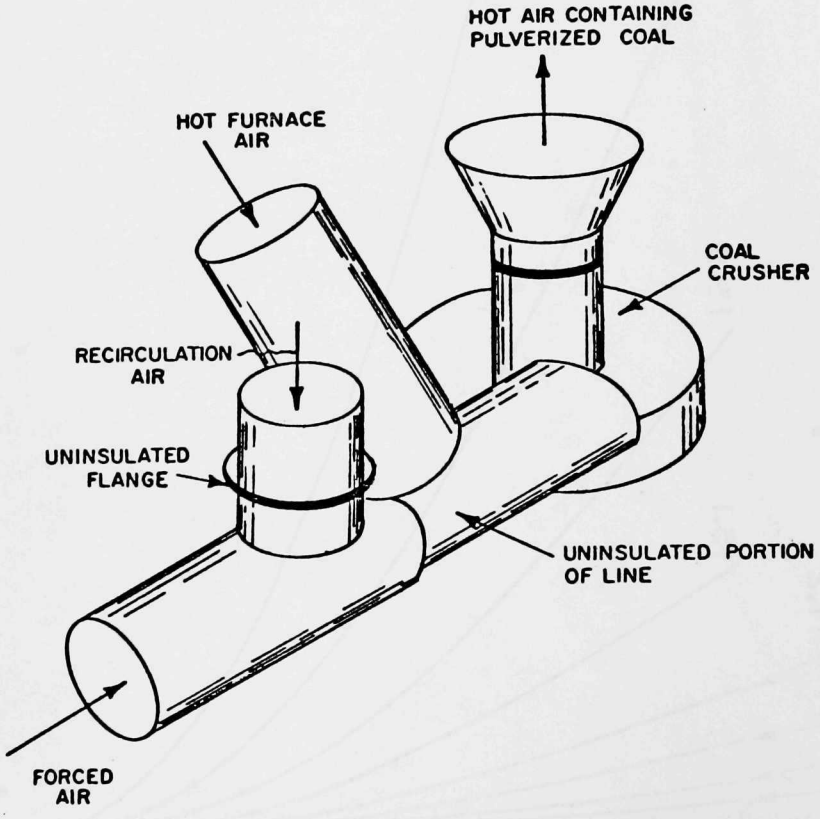

Fig. 5b. Line Drawing of Region Scanned with Infrared Camera

was concerned mainly with the gasifier and combustor vessels, although radiographs of transfer lines, distributor plates, and expansion joints were also obtained.

Two sets of radiographs were taken on the combustor (see Fig. 6). One set covering approximately 45% of the circumference on the combustor was taken adjacent to the top flange. Mounting flanges did not permit the film cassettes to be attached at other locations. A second set of radiographs was taken 4 ft from the top flange and covered approximately 69% of the circumference. All 14 x 17-in. radiographs from the combustor showed the presence of a horizontal steel bar. Consultation with Battelle personnel revealed that these are vapor barriers installed by the fabricator. Vapor barriers are rings 3 by 3/8-in. with a cross section welded around the entire circumference. The purpose of the vapor barrier is to attenuate the gas flow between the refractory and the shell should cracking of the refractory develop. The barriers are welded on 24-in. centers, as shown in Fig. 7. The monolithic lining of the gasifier and combustor is cast of Babcock and Wilcox KAOTAB refractory. Since the KAOTAB refractory was cast, it was necessary to vibrate the refractory to eliminate air pockets. However, below the barrier, the radiographs indicated voids that were typically 1/4-in. and of various lengths. Table 1 lists the percentage of the width of each radiograph that had a detectable void.

The gasifier (see Fig. 8) also was radiographed using a 47 Curie-^{60}cobalt source. Two locations were checked; one position adjacent to the top flange and another 11 ft below the flange. A density difference of 1.7 was obtained between radiographs taken around the top flange and those taken 11 ft lower. A typical photographic density obtained in the upper flange was 2.5, whereas a typical photographic density of 0.8 was obtained on the lower section. All radiographic parameters were held

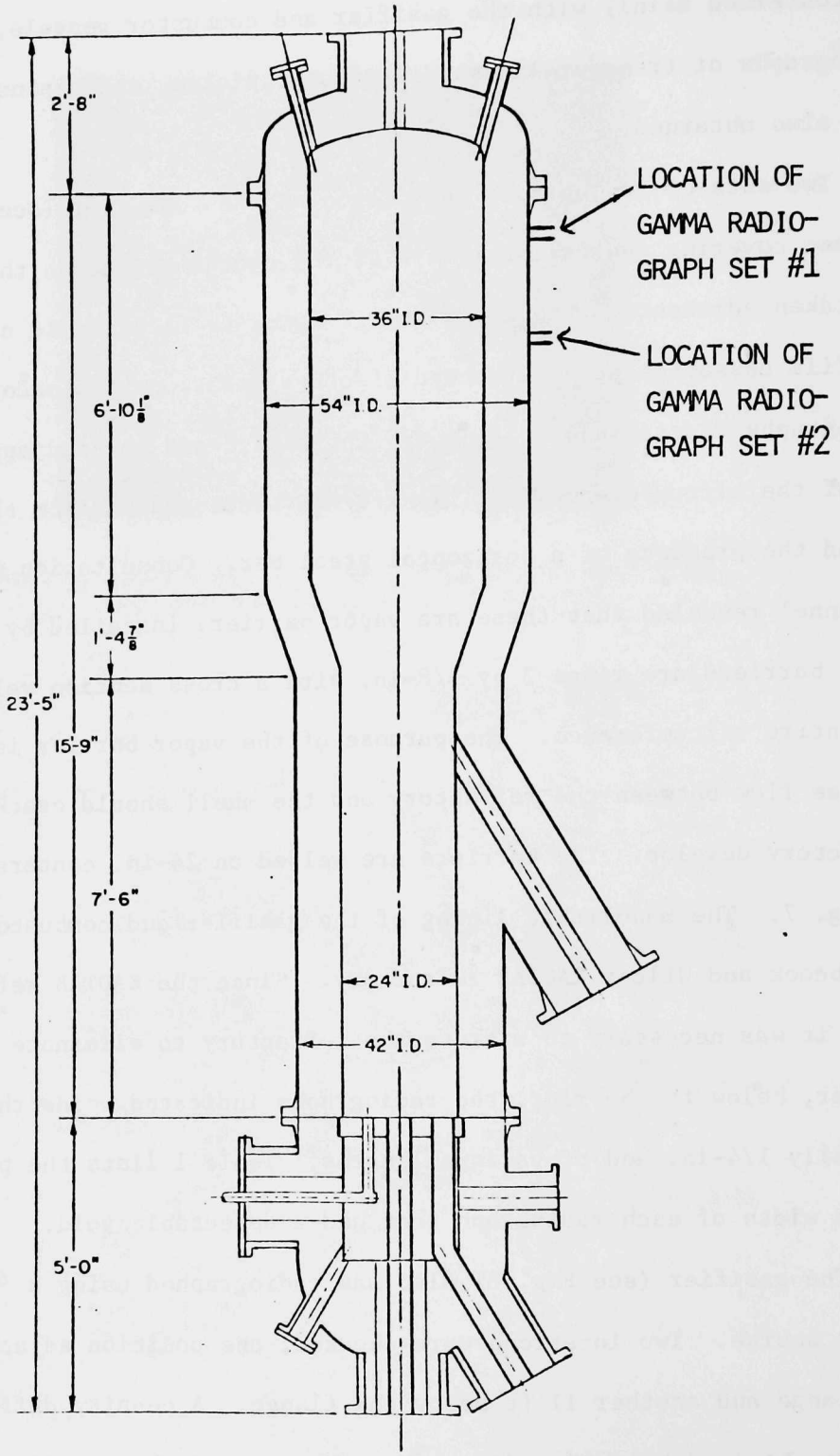

Fig. 6. Schematic of Combustor Vessel Used in Battelle Agglomerating Ash Coal Conversion Facility.

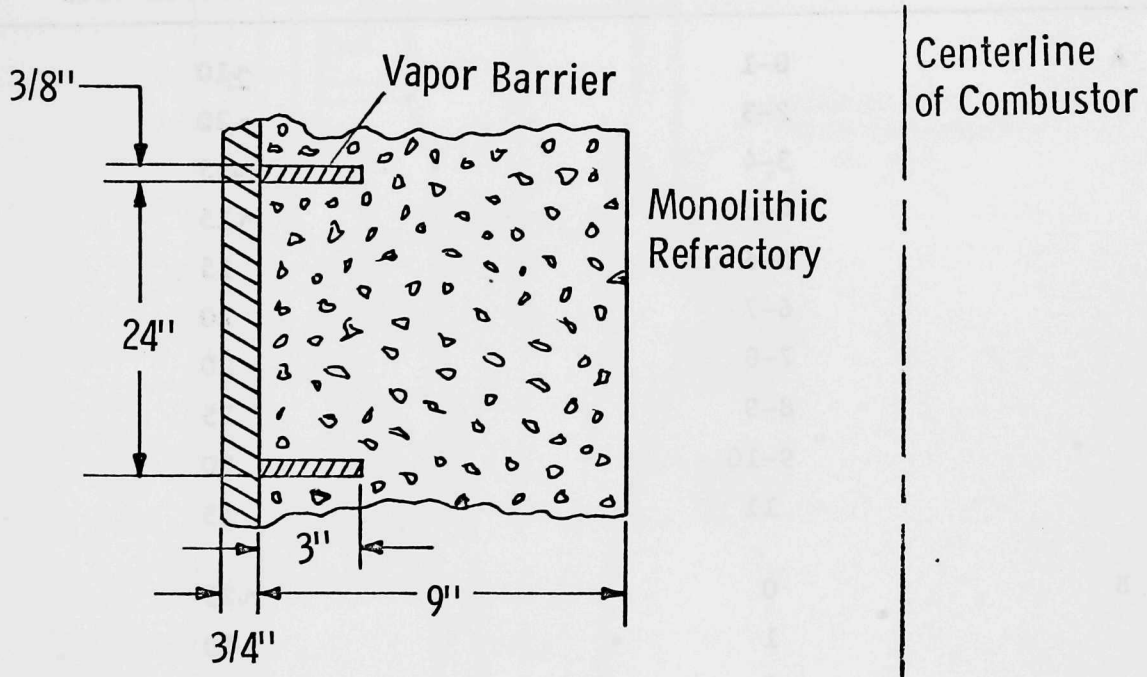

Fig. 7. Schematic of Vapor Barrier on Combustor Vessel.

Table 1. Apparent Void Percentage Below Vapor Barrier on Combustor.

Section	Radiograph	Percent of 14-in. Radiograph which Showed Void
A	0-1	~10
	2-3	~20
	3-4	~15
	4-5	~15
	5-6	15
	6-7	10
	7-8	20
	8-9	25
	9-10	50
	11	15
B	0	~25
	1	~50
	2	~35
	3	0
	4	~15
	5	~20
	6	~30
	7	~80

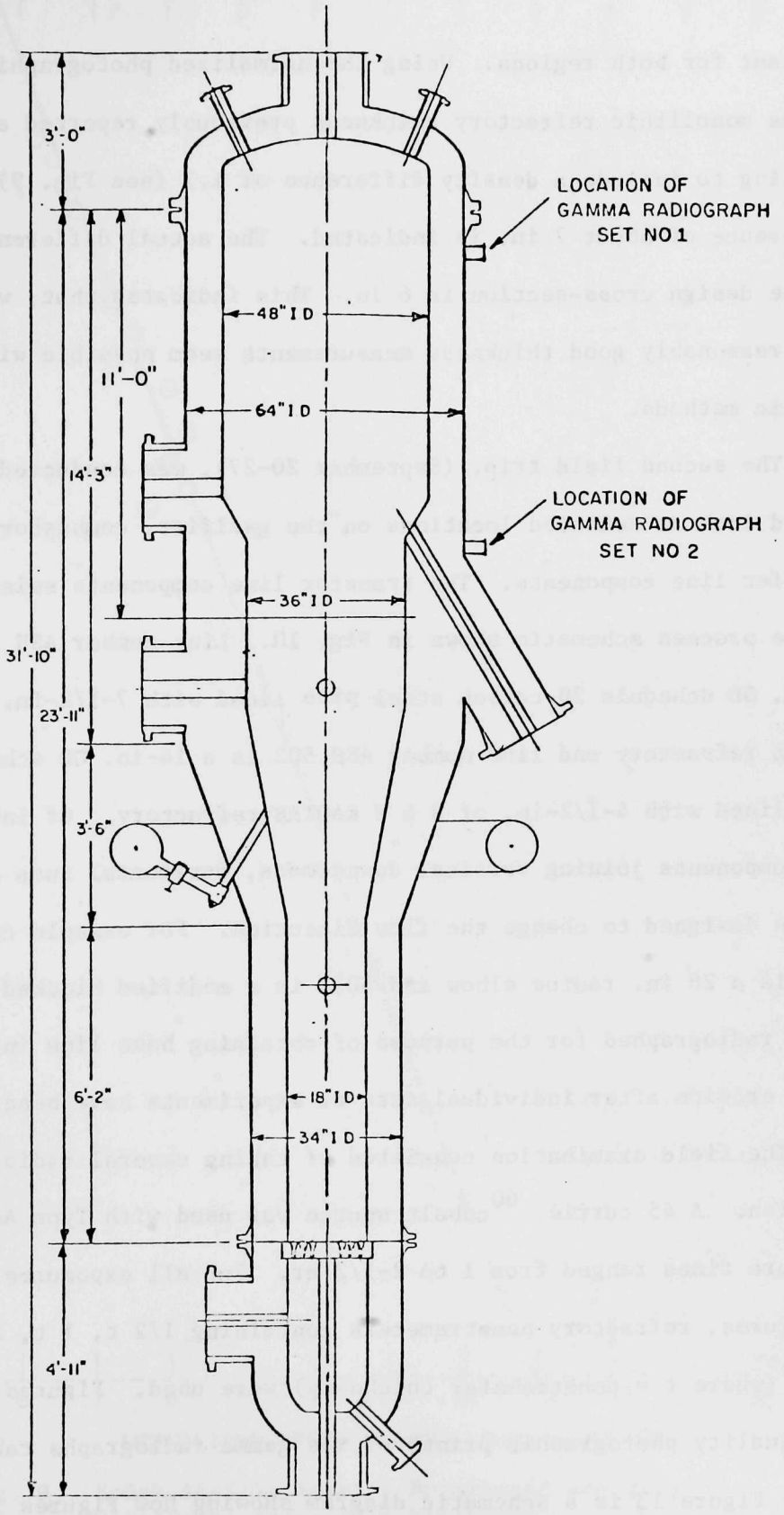

Schematic of Gasifier Vessel Used in Battelle Agglomerating Ash Coal Conversion Facility.

constant for both regions. Using the normalized photographic density versus monolithic refractory thickness previously reported and extrapolating to include a density difference of 1.7 (see Fig. 9), a thickness difference of about 7 in. is indicated. The actual difference, according to the design cross-section is 6 in. This indicates that, with additional work reasonably good thickness measurements seem possible with radiographic methods.

The second field trip, (September 20-27), was conducted to take a second look at selected locations on the gasifier, combustor, and critical transfer line components. The transfer line components selected are shown in the process schematic shown in Fig. 10. Line number ASH 501 is a 20-in. OD schedule 20 carbon steel pipe lined with 7-1/2-in. of B & W KOATAB refractory and line number ASH 502 is a 14-in. OD schedule 20 steel pipe lined with 4-1/2-in. of B & W KAOTAB refractory. Of interest were the components joining vertical downcomers, horizontal runs and vertical risers designed to change the flow direction. For example component 501A is a 28 in. radius elbow and 501B is a modified blocked "T". These were radiographed for the purpose of obtaining base line information to check erosion after individual sets of experiments have been conducted.

The field examination consisted of taking several radiographs at each location. A 45 currie ^{60}cobalt source was used with Type AA Kodak film. Exposure times ranged from 1 to 2-1/2 hr. For all exposures on layered structures, refractory penetrameters containing 1/2 t, 1 t, 2 t, and 3 t holes (where t = penetrameter thickness) were used. Figures 11 and 12 are high quality photographic prints of the gamma radiographs taken at location 502A. Figure 13 is a schematic diagram showing how Figures 11 and 12 relate to the elbow and flow direction. Note in Figs. 11 and 12 that dark region, which is

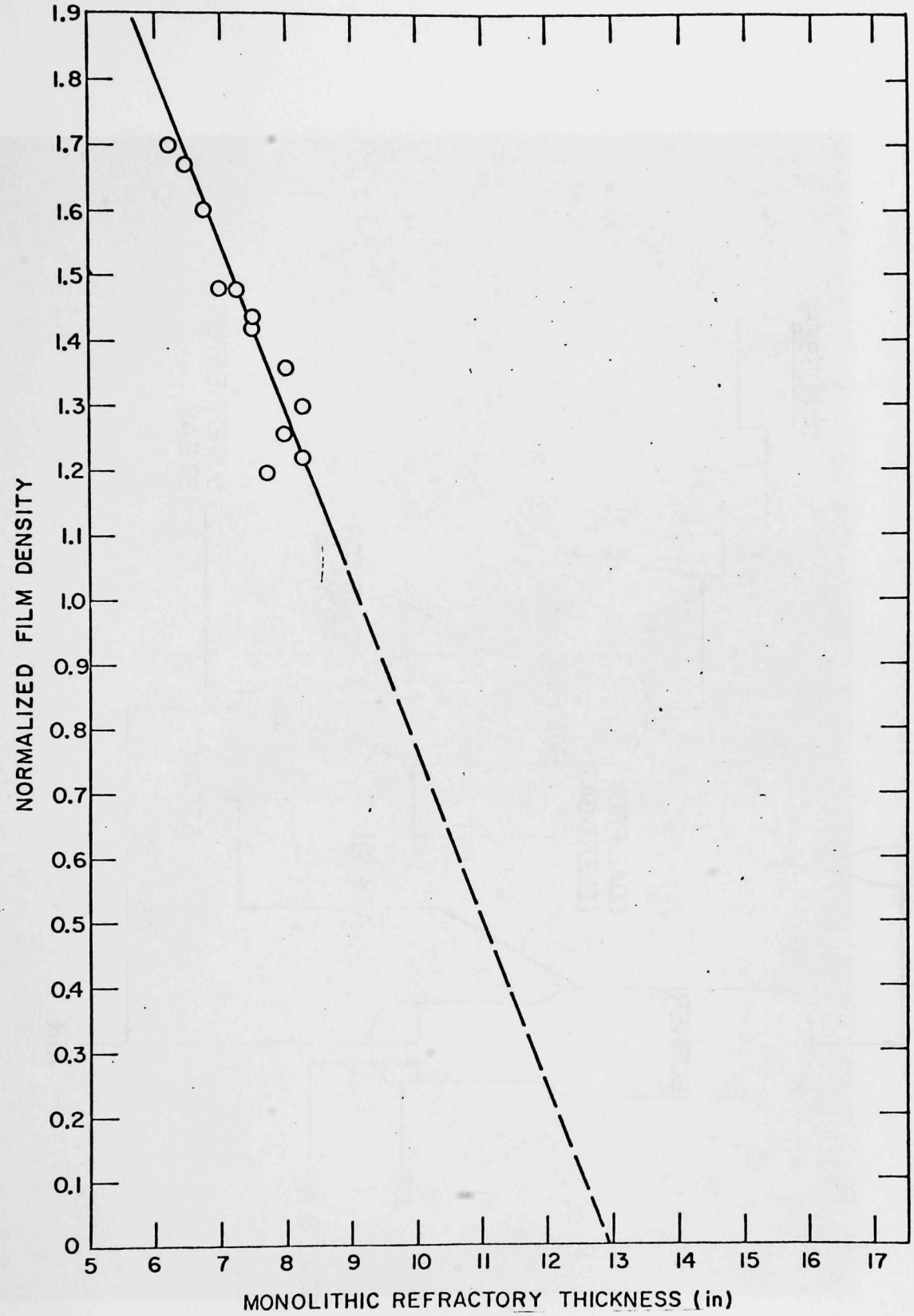

Fig. 9. Kodak AA-film Density Normalized and Related to Monolithic Refractory Thickness.

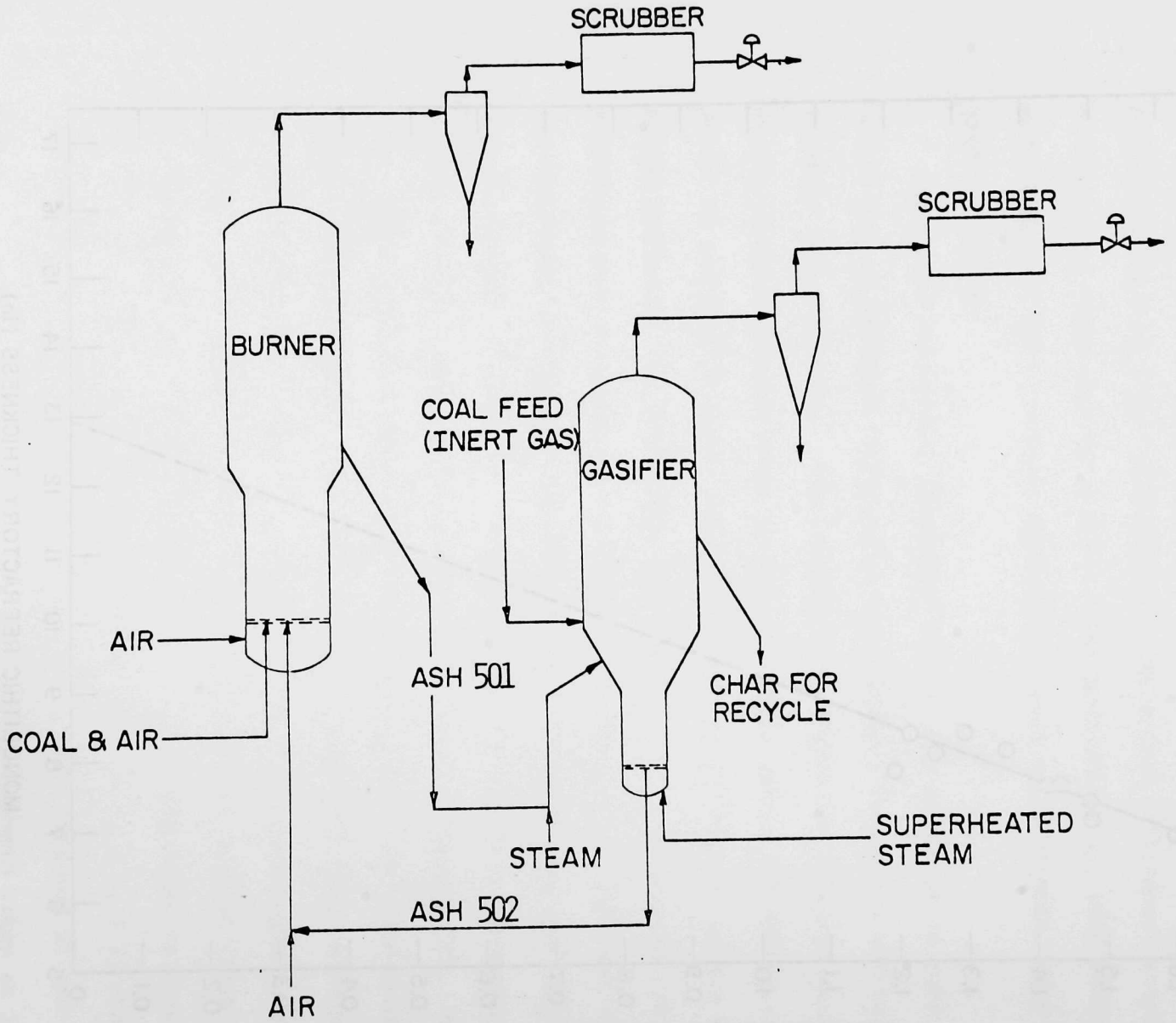

Fig. 10. Process Flow Diagram of Battelle Agglomerating Ash Process.

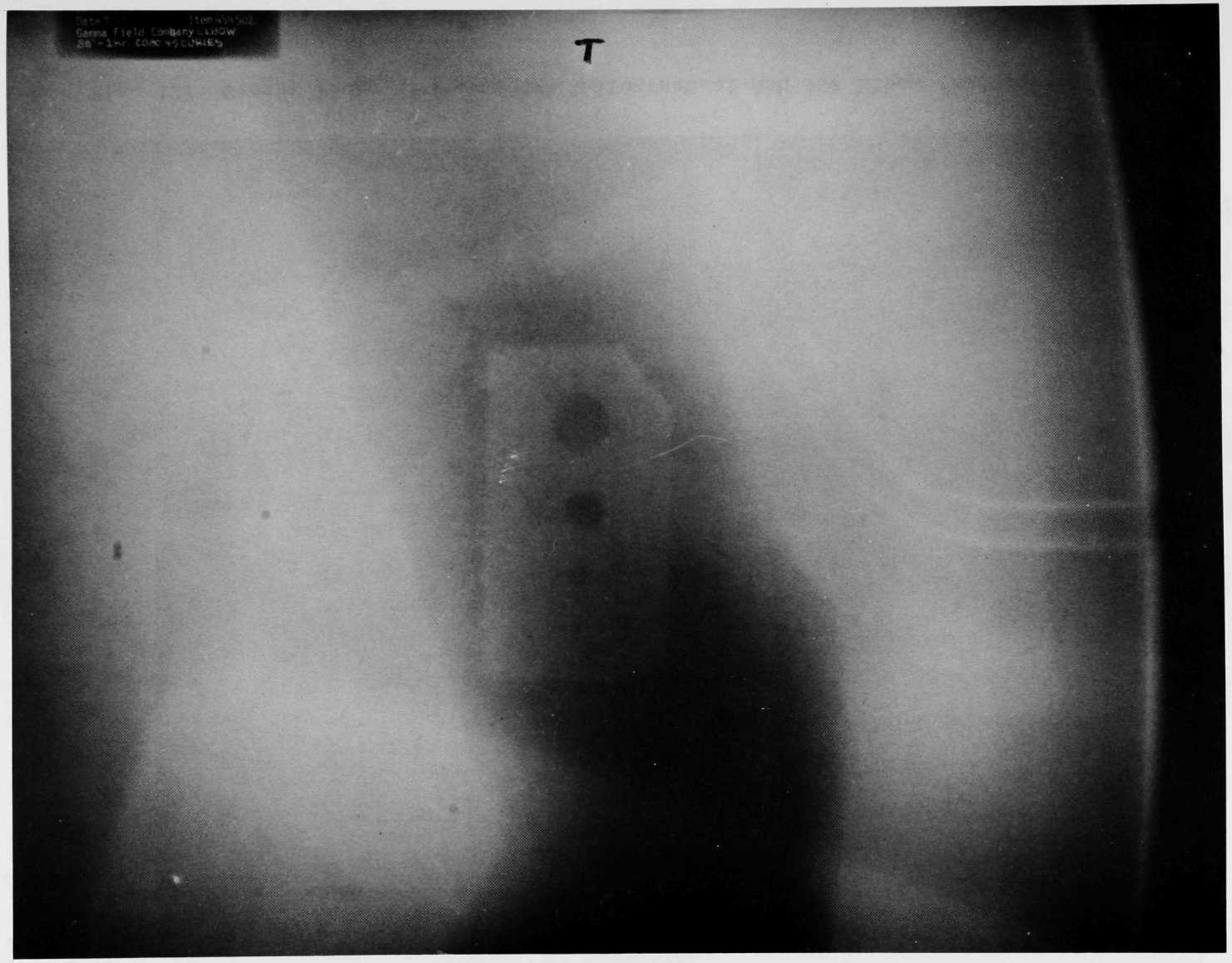

Fig. 11. Glossy Photo of Gamma Ray Radiograph of Ash 502 Elbow (Radiograph #1).

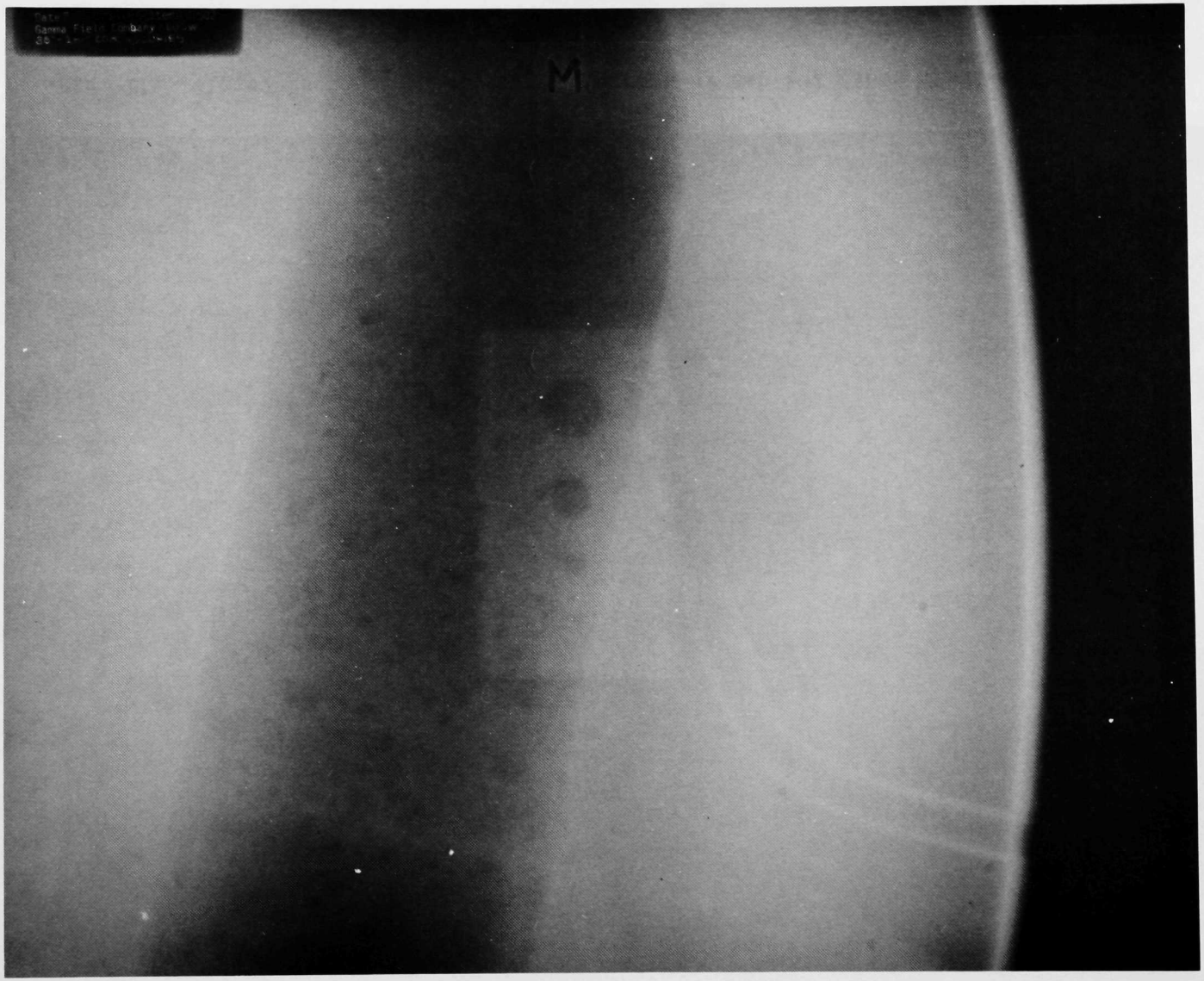

Fig. 12. Glossy Photo of Gamma Ray Radiograph of Ash 502 Elbow (Radiograph #2).

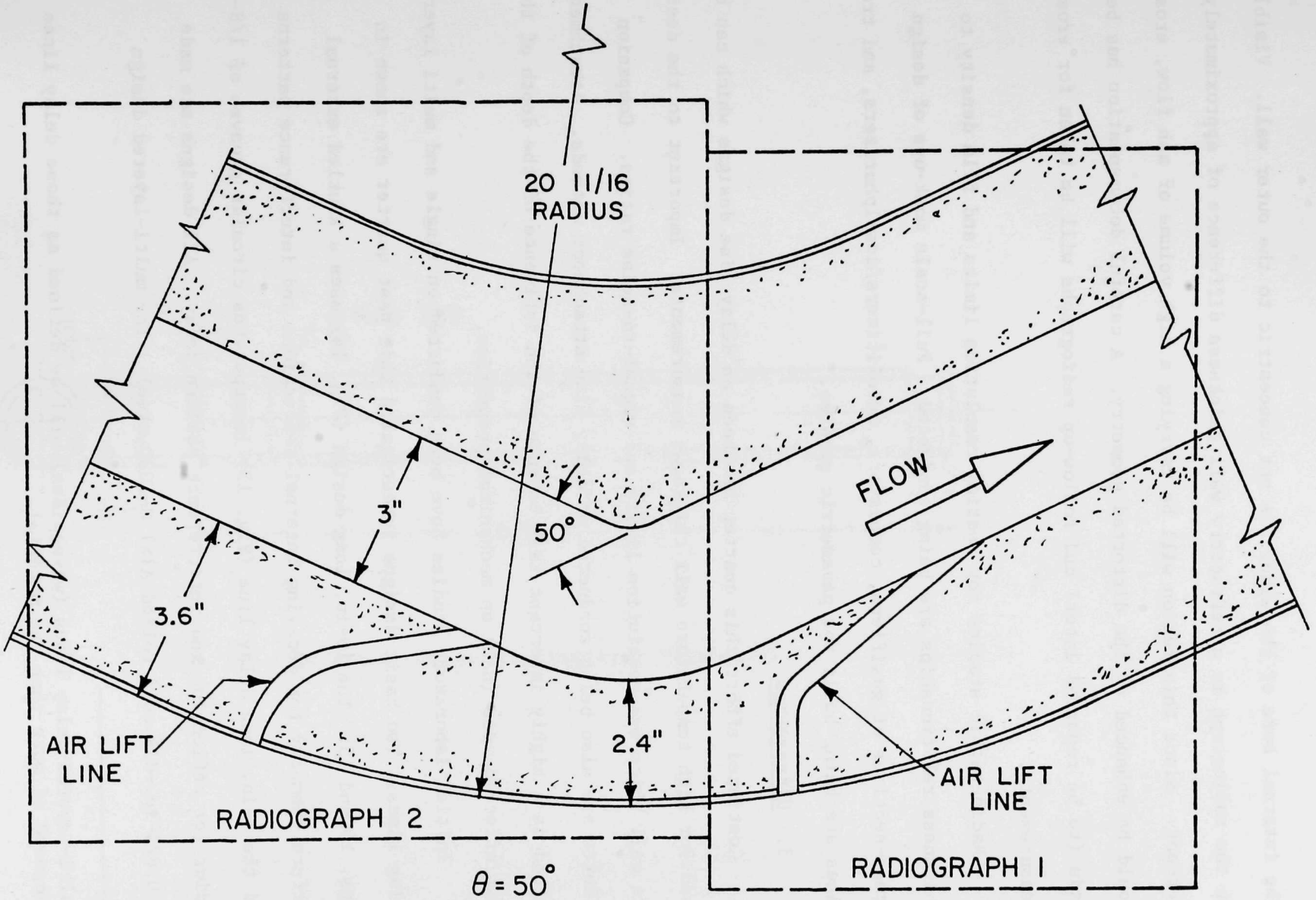

Fig. 13. Schematic Drawing Showing Relationship of Radiograph 1 (with Letter T on Top) to Radiograph 2 (with Letter M on Top).

the internal bore of the elbow, is not concentric to the outer wall. Visible on the radiograph is a refractory wall thickness difference of approximately 30 percent. Since this region will be carrying a high volume of ash flow, erosion could be enhanced by the distorted geometry. A careful documentation has been made (to be reported later) and follow-up radiographs will be taken for erosion measurements.

Radiographic studies for spatial resolution limits and film density to thickness relationships are being conducted. Full-scale mock-ups of design cross-sections of gasifiers, combustors, devolitizers/desulphurizers, and transfer lines are being built for parametric studies.

3. Ultrasonics

Continued effort this quarter has been on delay line designs which can be used for high temperature wall thickness measurements. Important to the designs are wall thickness resolution limits and signal-to-noise ratios. Companion efforts are also being conducted on delay line attachment methods. Attachment method is a highly important task because of the influence of the depth of the heat affected zone (HAZ) on mechanical properties.

Initial laboratory studies have been conducted on single and multi layer[a] delay lines. Two basic designs investigated this past quarter are shown in Figs. 14 and 15. The 10-in. long design (Fig. 14) uses a knurled external surface geometry for decaying internal reflections and interference patterns and the 6-in. long delay line (Fig. 15) incorporates circular grooves of 1/8-in. radius for reflection and interference pattern decay. All designs are made of 0.625-in.-dia cold rolled AISI C-1020 steel. The multi-layered design

---

[a]Multi-layered delay lines (waveguides) will be defined as those delay lines composed of more than one material.

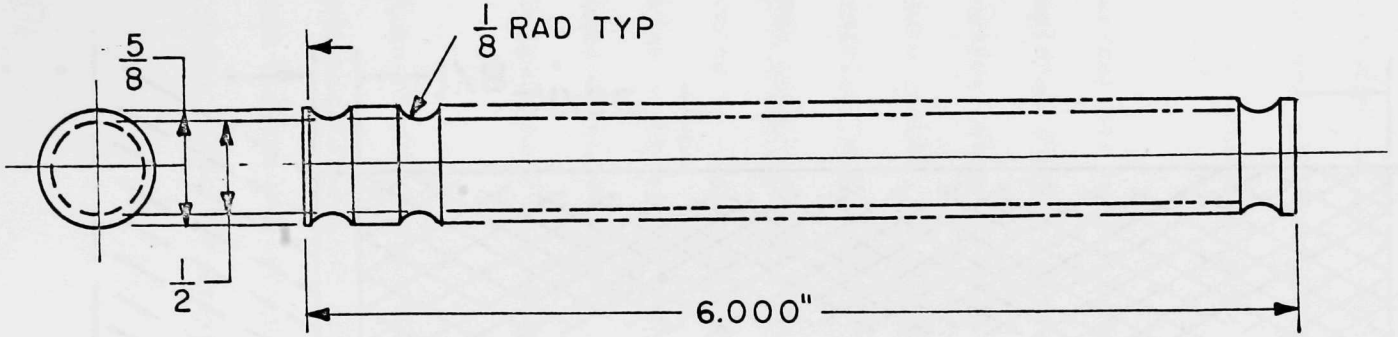

Fig. 14. Ultrasonic Delay Line Geometry (Design-2).

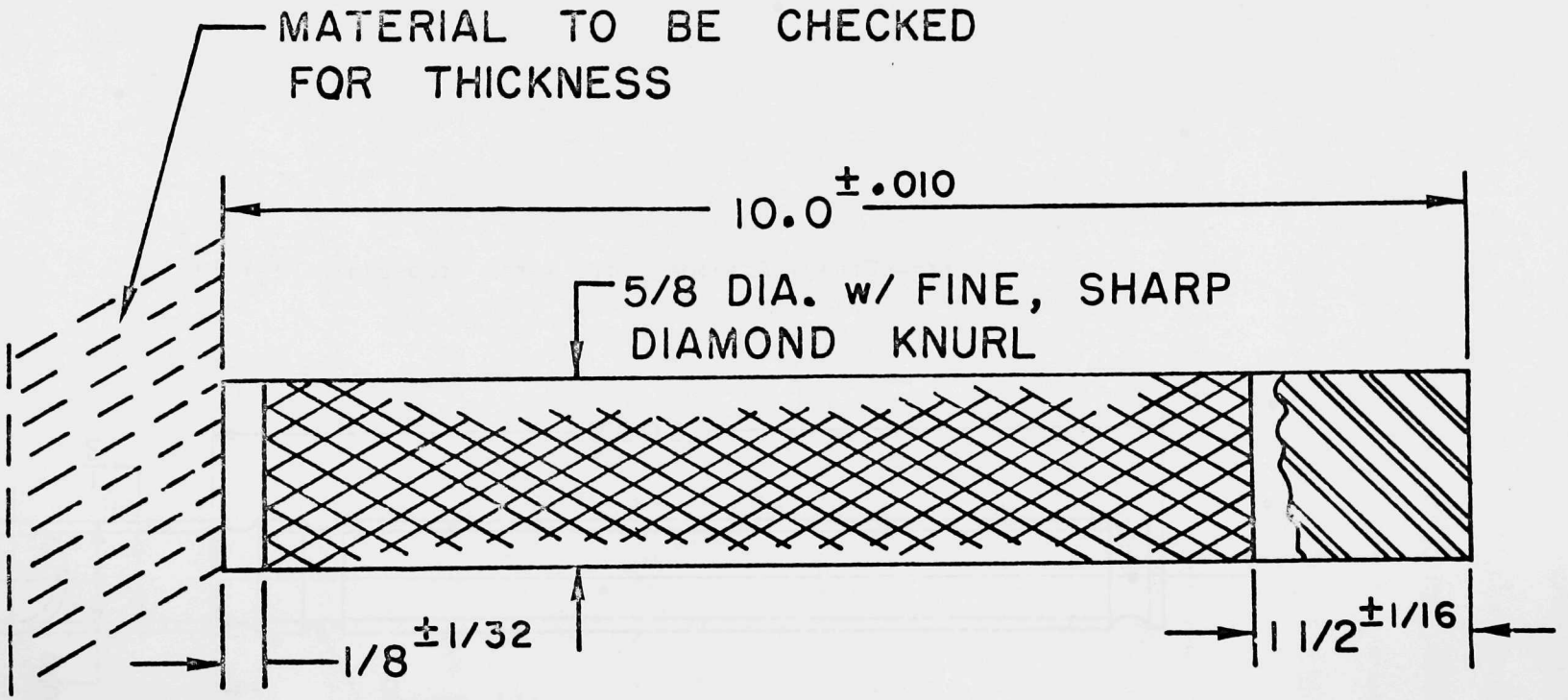

Fig. 15. Ultrasonic Delay Line Geometry.

incorporates a brass "lens" as shown in Fig. 16. All delay lines have been tested for signal-to-noise ratios using a repeatable dead load of about 340 grams. Table II lists the preliminary results of the laboratory tests.

A mock-up of the Bi-Gas product-gas/quench-section (see Fig. 17) has been constructed and is being studied for erosion points for wall thinning measurement locations. Initial through-flow tests with room temperature air and particulate matter indicates that the resulting erosion patterns on the Plexiglas can be used for ultrasonic wall thickness monitoring point locations.

4. Acoustic Emission

The single channel analyzer has been received and a two chamber pressurized system will be completed shortly for relating leak rate to acoustic emission. The laboratory device being built is shown schematically in Fig. 18. The acoustic emission pressure chamber and orifice plates should be completed by the end of October and initial leak rate testing begun.

5. Laboratory Apparatus Construction Status

The 3 by 4 by 2 ft furnace is about 50% complete and will be finished rapidly as soon as the heating elements arrive. Two gasifier design cross sections are in various stages of construction. One problem is obtaining the correct hangers. Special hangers have been designed and fabricated for most gasifier systems.

We have received drawings of the Petro-Carb slurry feed line at Synthane and construction of the instrumented section for erosion measurements has been initiated. This will include thermocouples, an array of high temperature wall thickness measurement delay lines for erosion monitoring.

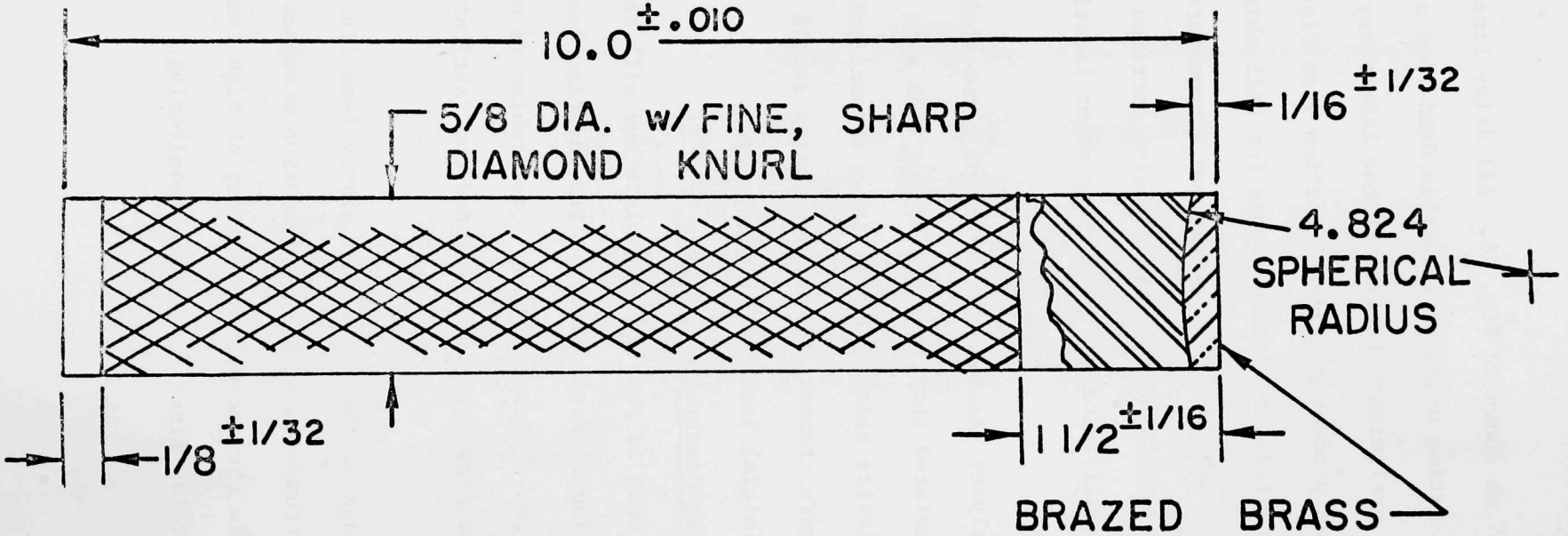

Fig. 16. Ultrasonic Delay Line Geometry Using Multi Layer Design.

TABLE II.

Waveguide Length in.	External Surface Distortion	Single or Multi Layered	Ultrasonic Transducer Freq (MH_z)/Size	S/N Ratio* Interface Pulse db	S/N Ratio* End of Rod Echo db
6	Grooved	Single Layer	5/1/4	6	11
6	Smooth	Single Layer	5/1/4	32	
6	Grooved	Single Layer	5/1/2	8	11
6	Smooth	Single Layer	5/1/2	45	
6	Grooved	Single Layer	10/1/2	2	7
6	Smooth	Single Layer	10/1/2	31	
10	Knurled	Single Layer	5/1/4	30	8
10	Knurled	Multi Layer	5/1/4	34	13
10	Knurled	Single Layer	5/1/2	45	19
10	Knurled	Multi Layer	5/1/2	46	16
10	Knurled	Single Layer	10/1/2	44	23
10	Knurled	Multi Layer	10/1/2	43	27

*The signal to noise ratios were determined by increasing the gain to bring the noise level up to the original signal level.

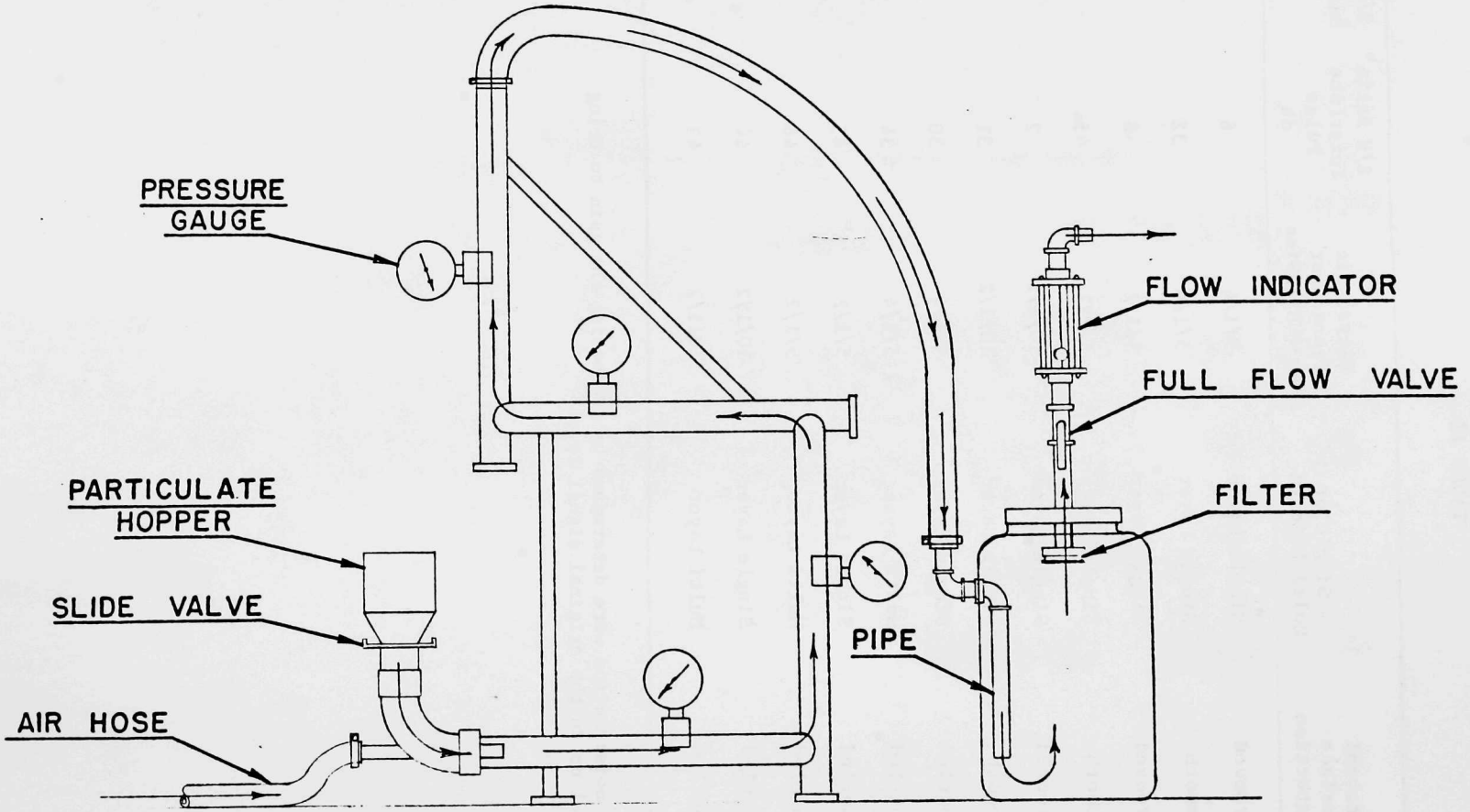

Fig. 17. Schematic of Bi-Gas Product Gas/Quench Section Flow Line.

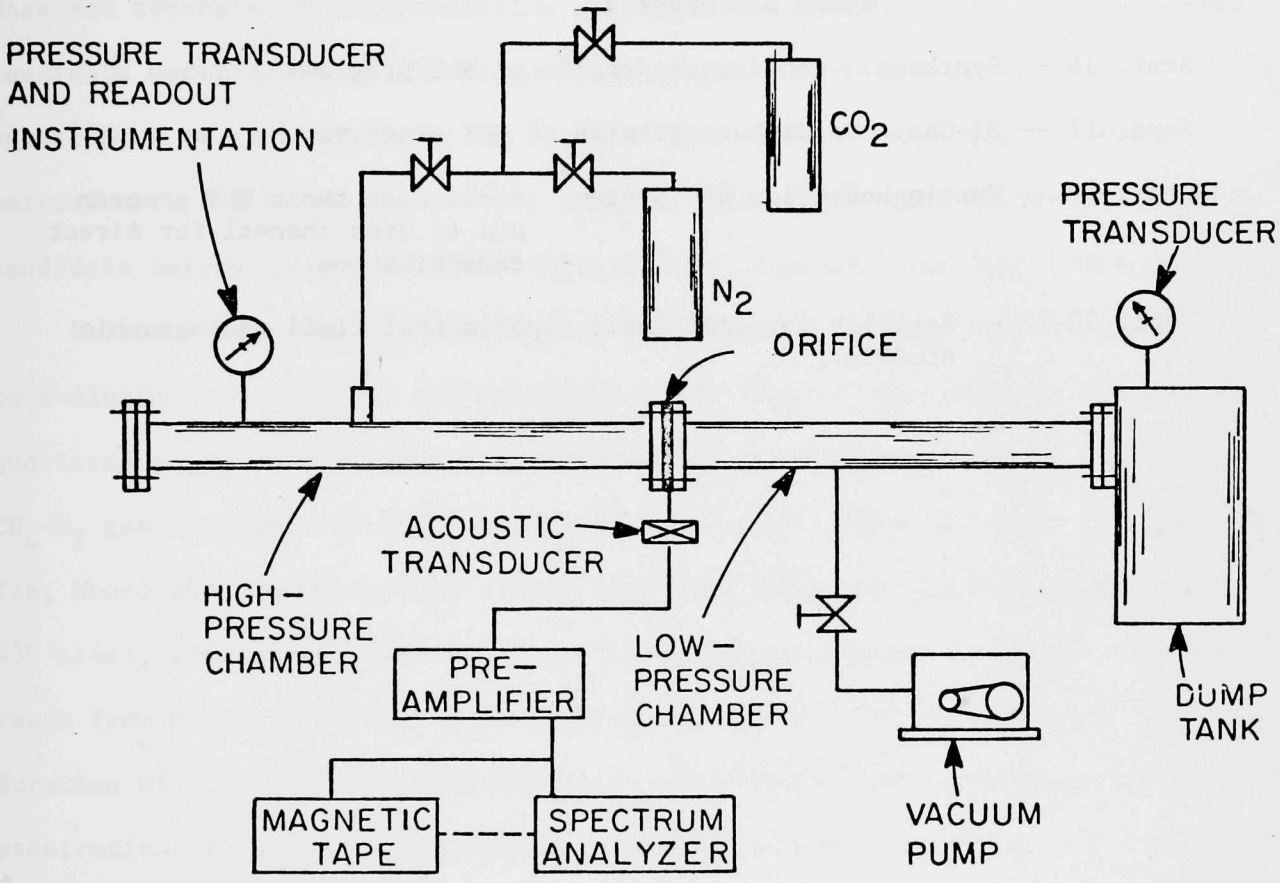

Fig. 18. Schematic of Acoustic Emission Leak Detection Set-up.

6. Field Visits this Quarter

July 10-11 -- CO_2: to perform initial infrared thermal studies

July 28 -- Hy-Gas: to discuss annual shut-down inspection.

July 29-31 -- Battelle: for field radiography studies.

July 31 -- Hy-Gas: to visually inspect reactor refractory cracking patterns and erosion.

Sept. 16 -- Synthane: to discuss details of NDT program.

Sept. 17 -- Bi-Gas: to discuss details of NDT program.

Sept. 19 -- Westinghouse low BTU System: to discuss their NDT program and to open channel for direct communication.

Sept. 20-27 -- Battelle for additional experimental field radiographic studies.

Task D: Corrosion Behavior of Materials in Coal-Conversion Processes.

(Principal Investigators: K. Natesan and O. K. Chopra)

The objectives of this subtask are to apply the available thermodynamic data and concepts to the prediction of probable corrosion reactions involving candidate materials over the range of temperatures and gas compositions anticipated in coal-gasification plants. This information, coupled with corrosion-rate data obtained under similar conditions, will be used to select candidate materials for further evaluation in simulated gasifier-plant conditions.

Existing high-temperature furnace and gas flow systems have been modified to evaluate carburization and oxidation resistance of materials in binary and quarternary gas environments. The carburization studies of 100 hr duration in CH_4-H_2 gas mixtures are being conducted with nickel-base (Inconels 600, 601, 625, 718, Monel 400) and iron-base (Types 304, 316, 309, and 310 stainless steel, 430 steel, and Incoloy 800) alloys. The carbon activities in these experiments range from 0.015 to 0.14 at a temperature of 875°C. Tests of 500 and 1000 hr duration will be conducted subsequently. The weight loss/gain and depth of penetration of carbon in the tested specimens will be evaluated. The specimens will also be examined by scanning electron microscopy and electron microprobe to evaluate the type and amount of precipitates that form in different materials as a function of temperature and gas composition. The data from this program will be used to develop analytical expressions for different corrosion processes.

TASK E: Erosion Behavior of Materials in Coal-Conversion Processes

(M. M. Mamoun)

The continuing analytical studies on material loss in an erosive-corrosive environment are presently considering erosive wear resulting from oblique impact. The main objective of these studies is to develop analytical models to reasonably predict the material loss and degration of mechanical properties of components utilized in coal gasification plants. These investigations are attempting to determine the effects on erosive wear of such quantities as the impact velocity, the angle of impingement, the size and shape, the mass density, the mass flux, and the gravimetric level or concentration of the eroding particles. Also, these studies consider the effects on erosion of such factors as the material properties of both the impacted components and the eroding particles, the operating temperatures, and the mechanical properties of the developed surface layers. The analytical formulations consider both ductile solids and brittle solids.*

Computer programs are being formulated to theoretically predict material loss rates by erosion. These programs currently are being developed for the following cases:

---

*In coal gasifiers the impact velocity of the eroding particles of coal, ash, slag, etc. does not, usually, exceed 150 ft/s; thus, the response of the eroded solid surfaces is quasi-static. This suggests that the rates of strain arising with impact are generally low. This and the high operating temperatures in coal gasifiers indicate that the metallic structures may experience relatively large plastic strains before fracture and hence are classified as ductile solids. Materials such as refractory ceramics however would undergo nominally elastic deformations until fracture, and hence are classified as brittle solids.

(a) Ductile metals subjected to normal impact velocities that result in nominally elastic deformations.

(b) Fully work-hardened ductile metals subjected to normal impact velocities that result in fully plastic deformations.

(c) Strain-hardening ductile metals subjected to normal impact velocities resulting in fully plastic deformations.

(d) Brittle solids subjected to normal impact velocities less than those necessary to cause surface macrocracks to develop;

(e) Brittle solids subjected to normal impact velocities causing macrocracks to develop on the impacted surface of the eroded component.

These programs take into account most of the erosion conditions that arise in coal gasification systems.

One of the purposes of these studies is to utilize the analytical results to formulate and conduct critical erosion experiments. The numerical results will then be compared with the experimental data to establish the validity of the theoretical assumptions. To conduct the experimental program, an experimental testing apparatus has been designed to simulate the erosive-corrosive conditions of a coal gasifier vessel.

A description is given in the following section of the testing apparatus design and some of the recent analytical results.

A. Description of the Proposed Erosion-Corrosion Experimental Investigation

The apparatus has been designed with several unique features and capabilities. Schematics of the apparatus are shown in Figures 1 and 2. Figure 1 shows schematically a pressure chamber into which preheated corrosive gases flow under

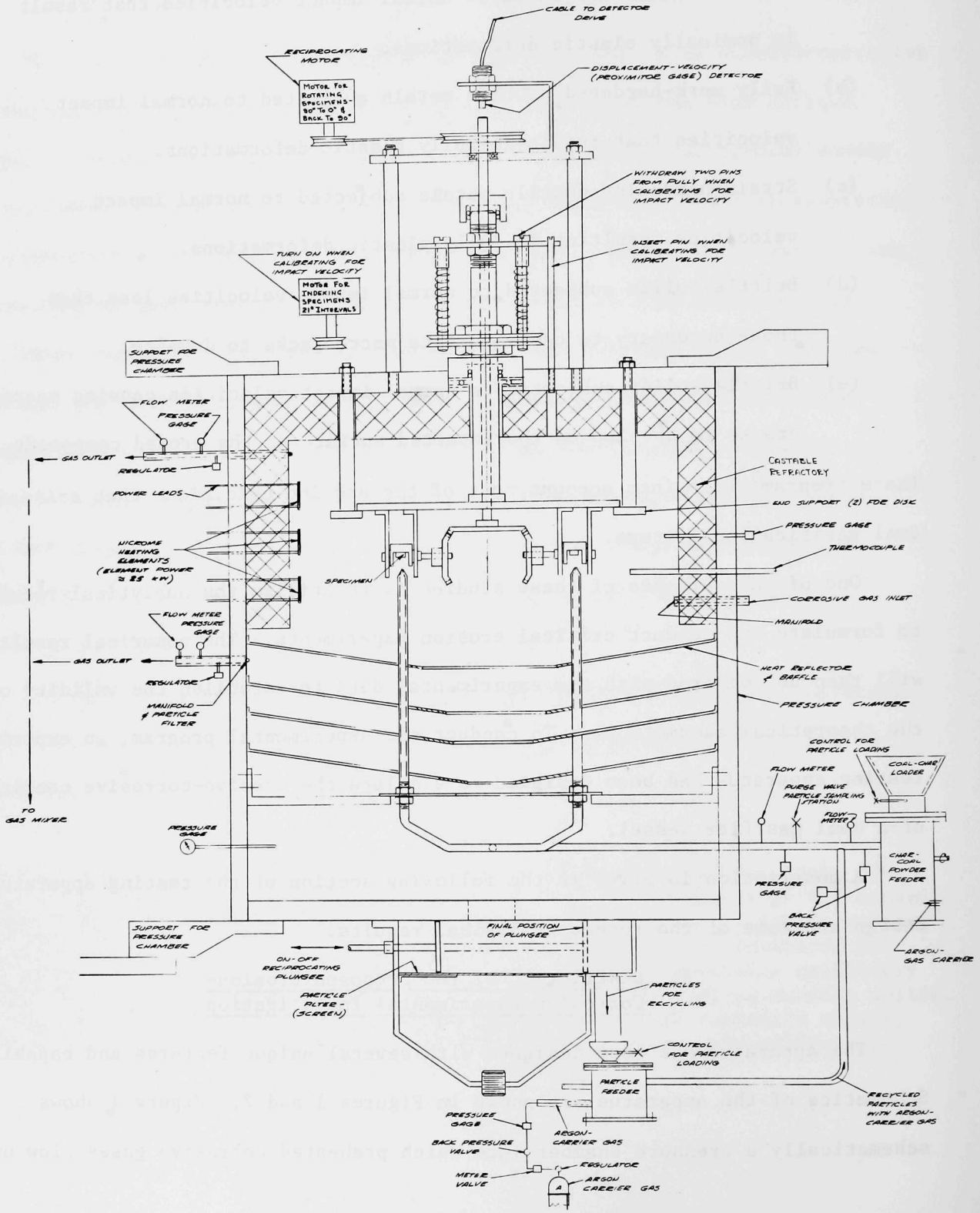

Figure 1. Schematic Illustration of the Multi-specimen Erosion-Corrosion Testing Apparatus.

ITEM	DESCRIPTION	Nº REQD
1	TEST SPECIMEN	16
2	BOLT - CRADLE	64
3	SHIELD - CRADLE	16
4	PIN - CRADLE - ROTATION AXIS	32
5	END - BRACKETS OF CRADLE	32
6	BUSHING - CRADLE	32
7	SUPPORT BRACKETS FOR CRADLE	32
8	NUTS - PIN CRADLE	32
9	BEVEL GEAR - DRIVEN	16
10	BEVEL GEAR - DRIVING	1
11	SHAFT - DRIVING BEVEL GEAR	1
12	SHAFT - DISK	1
13	DISK - FOR SPECIMEN SUPPORT & INDEXING	1
14	BLOCK - CRADLE	16
15	NOZZLE	16
16	NUTS - NOZZLE	32
17	DISK - FOR NOZZLE SUPPORT	1

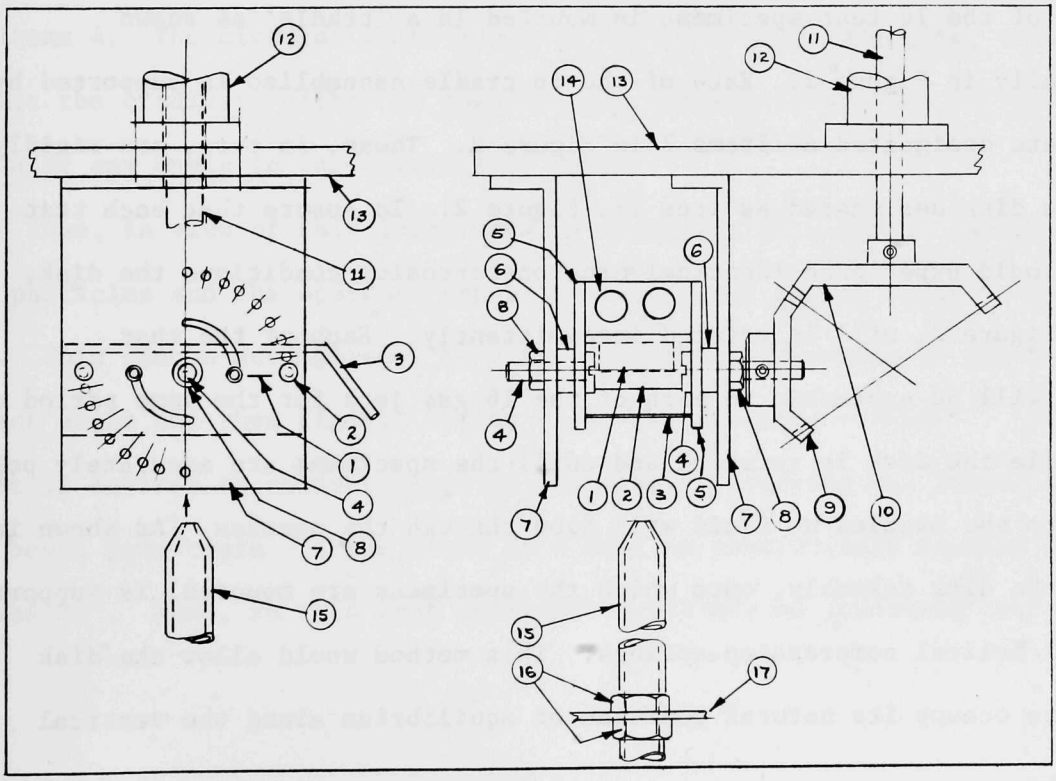

Figure 2. Schematic Illustration of the Cradle Assembly Used for Mounting a Test Specimen.

pressure. The weight percentages and the chemical constituents of the corrosive gases will be similar to those found in coal gasifiers. The test chamber will be insulated and heated by several rigidly mounted nicrome heating elements. As indicated in Figure 1, 16 metallic and/or ceramic specimens may be tested simultaneously and continously for a period not to exceed 20 hours. The eroding particles of ash, char, coal, dolomite, etc. are carried by the gas jets flowing through each of the 16 nozzles. The carrier gas in which the eroding particles are entrained is preheated Argon gas. The volumetric flow rate of the corrosive gases and the Argon particle-carrier gas will be controlled and varied. The rate of loading and the mass flux of the eroding particles can be accurately varied.

Each of the 16 test specimens is mounted in a 'cradle' as shown schematically in Figure 2. Each of the 16 cradle assemblies is supported by two brackets designated as items 7 in Figure 2. These, in turn, are rigidly fixed to a disk designated as item 13, Figure 2. To ensure that each test specimen would experience identical erosion-corrosion conditions the disk, item 13, Figure 2, will be rotated intermittently. Each of the test specimens will be subjected to each of the 16 gas jets for the same period of time. While the disk is rotating and until the specimens are accurately positioned relative to the nozzles no fluid will flow through the nozzles. As shown in Figure 1 the disk assembly, onto which the specimens are mounted, is supported by several helical compression springs. This method would allow the disk assembly to occupy its natural position of equilibrium along the vertical

direction. Due to impact, the eroding particles would cause the disk assembly to vibrate vertically relative to its position of equilibrium. The velocity of this vertical vibratory motion will be determined by using a velocity transducer - a Proximitor Gage - as shown schematically in Figure 1. This vibratory velocity will be employed for calibrating and determining the velocity of the eroding particles at the instant of impact.

A second method for measuring the impact velocity will also be used. This will consist of mounting externally the appropriate ultra-sonic devices on the shaft designated as item 11 in Figure 2. Figure 2 shows schematically the cradle assembly used for mounting the specimen designated as item 1. As can be seen, the cradle assembly is designed in such a manner so as to provide it with a degree of rotational freedom about the axis of the supporting pins designated as items 4. The circular slots shown in the supporting brackets, items 7, would permit the cradle to either be continuously rotated from 0° to 90° or to be rigidly fixed at any angle in the interval 0° to 90°.

Thus, in view of this latter design feature, the angle of impingement between the particles and the specimen can be set and fixed at any value between 0° and 90°. This can be accomplished by simply rotating the cradle to the desired impact angle and then rigidly fixing it to the brackets - items 7. Furthermore, if it is desired to conduct tests by continuously varying the impact angle then the bevel gear train - items 9 and 10 - will be continuously rotated between 0° and 90°. Thus, in this test apparatus tests may be conducted either at a

fixed impact angle or under a variable impact angle. In this testing apparatus both the corrosive gases and the eroding particles of ash, char, and dolomite can be continuously recirculated; this feature would facilitate continuous testing of up to 20 hours. Furthermore, the proposed testing apparatus would permit one to readily determine the frictional resistance developed between the eroding particles and the eroded surface. The latter information would provide some information on the properties of the surface films and thus would allow one to account for the surface films developed in the corrosive environment of coal gasifiers.

To summarize, the proposed testing apparatus designed for experimentally investigating the amount of material loss due to the erosive-corrosive environment of coal gasifiers would enable one to:

(1) Test 16 specimens simultaneously thus reducing the total time required to conduct critical experiments.

(2) Conduct continuous test runs for a period of about 20 hours; this would ensure the generation of data under steady state conditions and thus would enable one to reliably predict the erosion behavior of materials subjected to relatively long operating duration.

(3) Vary, control, and measure the impact velocity of the eroding particles.

(4) Select, vary, and control the impact angle.

(5) Vary, control, and measure the rate of loading and the mass flux of the eroding particles.

(6) Vary and control the volumetric flow rate and the flow velocity of the particle-carrier gas.

(7) Change and control the chemical constituents, and the volumetric flow rate of the corrosive gases.

(8) Vary and control the operating temperature.

(9) Vary and control the operating pressure.

(10) Measure the frictional resistance of the various surface layers.

Initially, the proposed testing program will investigate the effects of some of the variables as described in Table I.

The analytical investigations indicate that experimental studies should be conducted to determine the effects of the erosive-corrosive environment of coal gasifiers on:

(1) Variation in hardness with depth.

(2) Changes in dimensions, weight, and surface finish of eroded surface.

(3) Changes in eroding-particle size and configuration.

(4) Dimensions and distribution of surface flaws.

(5) Subsurface transformation.

(6) Yield and ultimate strengths and the fracture stress of the eroded surface.

(7) Modulus of elasticity and Poisson's ratio of the eroded surface.

The experimental work will, therefore, be directed so that the effects of erosion-corrosion on the quantities and properties can be assessed and evaluated.

B. Description of Some of the Results of the Continuing Analytical Modeling Studies

To develop useful and meaningful analytical models for the erosive-corrosive behavior of components used in coal gasification plants, it is necessary to determine the stress fields and types of deformations that can cause material loss. Furthermore, it is essential to determine: the range of impact velocities

TABLE 1. POSSIBLE TESTS

(5) IMPACT SPEEDS (m/s)	(6) IMPACT ANGLES	(3) PARTICLE SIZES	(3) PARTICLE MATERIALS	(4) PARTICLE LOADINGS
1	15°	$1(10^{-4})$m ≡ 100 μm ∿150 MESH	Coal-Char-Ash	0.47 Kg/am^3 (≈0.3 Lb/100 acF)
5	25°	$4(10^{-4})$m ≡ 400 μm ∿40 MESH	SiO_2	1.88 Kg/am^3 (≈1.2 Lb/100 acF)
10	40°	$8(10^{-4})$m ≡ 800 μm ∿-20 MESH	Steel	7.5 Kg/am^3 (≈4.8 Lb/100 acF)
20	60°			15 Kg/am^3 (≈9.6 Lb/100 acF)
40	80°			
	90°			

(2) VOLUMETRIC FLOW RATES OF CARRIER FLUIDS	(3) MASS FLUX OF ERODING-ABRADING PARTICLES	(5) EROSION DURATION PERIOD	(8) IMPACTED MATERIALS (SUBSTRATES)
1.415 acm/hr (= 50 acf/hr)	$3(10^{-2})$ g/cm^2/s	5 min	AISI 4340 (HARD)
2.830 acm/hr (= 100 acf/hr)	3 g/cm^2/s	30 min	AISI 304 (HARD)
	30 g/cm^2/s	1 hr	AISI 310 (ANNEALED)
		2 hrs	INCONEL 600
		5 hrs	CERAMICS, OTHERS (4)

(4) TEMPERATURES	(2) ENVIRONMENT	(2) PRESSURES	(3) REPEATABLE TESTS
RT	ROOM	$1.01(10^5)$ N/m^2 (≈14.7 psi)	3 DATA POINTS PER TEST
148°C (≈300°F)	CORROSIVE	$3.44(10^5)$ N/m^2 (≈50 psi)	
538°C (≈1000°F)			
982°C (≈1800°F)			

of the eroding particles that cause various modes of deformations to occur; the thickness of surface layers that undergo cumulative plastic strains, or the extent of the region where the fracture stress is exceeded; and the volume of material in which such a critical state is reached. The current studies are directed at these questions. Some of the results of the analytical formulations follow.

Mathematical expressions have been developed for determining the magnitude V_{ip} of the minimum impact velocity of the eroding particles that is required to cause an impacted surface of a ductile metallic solid to flow plastically. These expressions are derived in terms of the impingement angle α, the material properties of both the eroding particles and the impacted surface, and the sliding friction coefficient f, which is a measure of the mechanical properties of the developed surface layers of oxides, sulfides, etc. These expressions are found for two cases as follows:

case (a): Nonstrain-hardening Ductile Metals

$$V_{ip} = \left\{ \left(\frac{25\,\pi^2}{6\sqrt{3}} \right) \left(\frac{3}{2\,\rho_1\,p_{fn}} \right)^{1/2} \left[\left(\frac{1 - \nu_1^2}{E_1} \right) + \left(\frac{1 - \nu_2^2}{E_2} \right) \right]^2 \left(\frac{Y_{d2}}{F_y} \right)^3 \left(\frac{1}{\sin \alpha} \right) \right\}. \tag{1}$$

case (b): Strain-hardening Ductile Metals

$$V_{ip} = \left(\frac{1}{\sin \alpha} \right) \left\{ \left(\frac{25\,\pi^2}{3\sqrt{3}} \right) \left[\left(\frac{1 - \nu_1^2}{E_1} \right) + \left(\frac{1 - \nu_2^2}{E_2} \right) \right]^2 \left(\frac{Y_{d2}}{F_y} \right)^3 \right\}^{(4 + n_o)/2(2 + n_o)} \Bigg/$$

$$\left[(0.2)^{2\,n_o/(2 + n_o)} \,(4 + n_o) \left(\frac{2\,\rho_1}{3} \right) (c\,B_o)^{2/(2 + n_o)} \right]^{1/2} . \tag{2}$$

The approximate value of the function F_y may be computed from

$$F_y \approx \left[0.066\ (1 + \nu_2)^2 - 0.357\ (1 + \nu_2) + 0.48\right]^{1/2},$$

for $f = 0$ and/or $\alpha = 90°$;

$$F_y \approx \left\{\left[0.066\ (1 + \nu_2)^2 - 0.357\ (1 + \nu_2) + 0.48\right]^{1/2} + 0.104\ f\right\},$$

for $0 < f < 0.27$, and

$\alpha < 90°$;

$$F_y \approx \left\{\left(\frac{1}{3}\right)\left[\left(\frac{\pi f}{8}\right)^2 (16 - 4\nu_2 + 7\nu_2^2) + \left(\frac{\pi f}{4}\right)(2 - 5\nu_2 + 2\nu_2^2) + \left(\frac{1}{3}\right)(1 - 2\nu_2)^2\right]\right\}^{1/2}$$

for $f \geq 0.27$ and $\alpha < 90°$. (3)

Here, the following notation has been used:

V_i = magnitude of the velocity of the eroding particles at first instant of impact,

V_{ip} = magnitude of the minimum impact velocity necessary for fully plastic deformations or cumulative plastic strains,

α = impingement angle,

E_1, E_2 = moduli of elasticity of the erodding spherical particle and the impacted flat surface, respectively,

ν_1, ν_2 = Poisson's ratios of the eroding particle and the impacted surface, respectively,

Y_{d2} = dynamic yield strength corresponding to 8% permanent strain of the impacted surface,

p_{fn} = plastic flow pressure or stress of impacted surface in case it is non-strain hardening; or a representative value of the plastic flow stress in case the surface strain hardens,

n_o = strain-hardening exponent of impacted metallic surface,

ρ_1 = mass density of the eroding particles,

c = a constant whose value is ~ 3,

B_o = yield stress corresponding to 100% strain,

= $S_{ut2}\,(e/n_o)^{n_o}$ where $e \approx 2.718$ is the natural logarithmic base, and

S_{ut2} = ultimate strength of the impacted surface.

It can be shown that in case the impacted surface is not chemically clean, then the approximate value of the friction coefficient f may be computed from[3]

$$f \approx \frac{S_c}{p_{fn}} + f_d \quad , \tag{4}$$

where S_c is the shear strength of the interfacial layer or film of oxide, sulfide, etc. that develops on the impacted surface, also, f_d is, in general, a function of the material properties and the geometry of the surface asperities. For the normal type of engineering surfaces the value of f_d is approximately 0.05. Here, p_{fn} pertains to the substrate of the impacted eroded surface. This may be evaluated for two cases as follows:

Case (a): Nonstrain-hardening Ductile metals

$$p_{fn} \approx c\, Y_{d2} \, . \tag{5a}$$

Case (b): Strain-hardening Ductile metals; here an average or representative value of the flow stress may be taken as:

$$p_{fn} \approx \left\{ \left(\frac{32}{3}\right)\left(10^{-4}\right)\left(c\ B_o\right)^{4/n_o} \left(4 + n_o\right) \rho_1 \left(V_i \sin \alpha\right)^2 \right\}^{n_o/(4 + n_o)} ,$$

for $V_i \geq V_{ip}$. (5b)

Consider the case of spherical particles of coal, char, and slag impacting a flat steel surface that is fully work-hardened and that has a yield strength of $Y_{d2} \approx 30{,}000$ psi $\approx 206.84\ (10^6)$ N/m^2. Using Eq. (1), and introducing several values for the coefficient of friction and the angle of impact, we get the numerical values for the magnitudes of the resultant impact velocities of the coal and slag particles that cause the steel surface to undergo full yielding and hence cumulative plastic strains; these values are given in Table 2.

Table 2. Minimum Magnitude of the Resultant Impact Velocity of Coal, Ash, and Slag Particles Required to Cause Fully Plastic Deformations in a Work-hardened Steel Surface Having a Yield Strength of 30,000 psi $\sim 2.068\ (10^8)$ N/m^2.

f	α, deg.	V_{ip}	
		ft/s	m/s
0	90°	12.9	3.93
0	85°	12.97	3.95
0	65°	14.25	4.34
0	45°	18.27	5.57
0	20°	37.78	11.51
0	10°	74.42	22.68
0.25	90°	12.9	3.93
0.25	85°	10.57	3.22
0.25	65°	11.62	3.54
0.25	45°	14.90	4.54
0.25	20°	30.8	9.39
0.25	10°	60.68	18.49
0.5	90°	12.9	3.93
0.5	85°	3.48	1.06
0.5	65°	3.83	1.16
0.5	45°	4.91	1.5
0.5	20°	10.16	3.1
0.5	10°	20	6.1

Equations (1) and (2) and the results given in Table 2 show that during erosion, full yeidling is adversely affected by environmental conditions which influence the degree of friction. As the friction between the obliquely impacting eroding particles and the eroded surface intensifies, full yielding of the eroded surface takes place at relatively low impact velocities. Thus, frictional shearing stresses arising during erosion greatly facilitate the development of fully plastic deformations and hence enhance the cumulative plastic strains leading to material loss.

When the magnitude of the resultant impact velocity attains a value equal to or greater than V_{ip}, relatively large permanent craters form in the impacted surface. This volume severs after a relatively small number of impacts. Hence, the material loss experienced by ductile members is much greater than that resulting from impact velocities causing only elastic deformations. The results given in Eqs. (1) and (2) indicate that in designing members to withstand an erosive environment materials and conditions should be chosen so as to maximize the normal component of V_{ip}, namely, the product (V_{ip} sin α). To maximize this latter quantity and hence to minimize the material loss, the Poisson's ratio and the moduli of elasticity of the eroding particles and the impacted surface, the mass density of the eroding particles, and the friction coefficient must have values as low as possible and the yield and ultimate strengths of the impacted surface must have values as large as possible.

2. Magnitude of the Minimum Oblique Impact Velocity of Solid Particulates Required For the Fracturing and Fragmentation of Brittle Solids Subjected to Erosive Conditions

As the eroding solid particles impinge on the surface of a brittle solid at sufficiently large impact velocities, microcracks may develop in the brittle solid leading to erosion. It can be shown that fracture and cracking of a flat surface of a brittle solid made from isotropic and homogeneous material commences when the magnitude of the resultant impact velocity of the eroding spherical solid particles is equal to or greater than a certain value V_{ic} given as:

$$V_{ic} = \left(\frac{\pi^4}{40}\right)^{1/2}\left\{\left[\frac{1-\nu_1^2}{E_1} + \frac{1-\nu_2^2}{E_2}\right]^2 \rho_1^{-1/2}\left(\frac{\sigma_{crit}}{F_c}\right)^{5/2}\left(\frac{1}{\sin\alpha}\right)\right\}. \qquad (6)$$

Here, the value of the function F_c may be found from

$$F_c = \left[\frac{(4+\nu_2)\pi f}{8} + \frac{(1-2\nu_2)}{3}\right], \text{ for } \alpha < 90°$$

$$= \left(\frac{1-2\nu_2}{3}\right), \text{ for } \alpha = 90°. \qquad (7)$$

Therefore, knowing the values of the material constants, the mass density of the eroding particles, the critical fracture stress, the friction coefficient, and the angle of impingement, the smallest magnitude V_{ic} of the impact velocity of the eroding particles that is required to initiate fracture may be calculated by using Eqs. (6-7). With brittle solids, if the impact velocity is less than V_{ic}, then the material loss due to erosion is less than that

resulting when the impact velocities are equal to or greater than V_{ic}. Since the normal velocity component at impact is equal to ($V_i \sin \alpha$), then the results given in Eqs. (6-7) show that for given materials and surface conditions, the normal velocity component is the dynamic quantity that determines the stage at which macrocracking and fragmentation of the impacted brittle solid takes place. These observations suggest that to minimize material loss experienced by brittle solids in an erosive environment, one must select design specifications in such a manner so as to maximize the value of the normal component of V_{ic}, namely, the product ($V_{ic} \sin \alpha$).

Inspection of Eqs (6-7) reveals that the product ($V_{ic} \sin \alpha$) increases with decreasing moduli of elasticity, mass density, and coefficient of friction and with increasing fracture or critical stress. The results also show that it takes less impact velocity to cause cracking and fragmentation at high impact angles than at low impact angles. Tables 3 and 4 give the numerical values of the magnitude of the minimum impact velocity of particles of coal, ash, char, and slag that is necessary for crack initiation in a flat martensitic steel structure; these values correspond to different coefficients of friction, impingement angles, and critical fracture stresses.

The numerical results given in Tables 3 and 4 demonstrate that during erosion brittle solids having relatively low fracture stress would fracture under low impact velocities. The results also indicate that in case the eroding particles impact a surface at an angle <90°, then any increase in the sliding frictional forces set-up between the eroding particles and the surface would greatly facilitate the cracking and fragmentation of the impacted brittle solid. This is due to the fact that when particles impact a surface obliquely,

Table 3. Magnitude of the Minimum Impact Velocity of Coal, Ash, and Slag Particles Required for the Cracking and Fragmentation of a Flat Martensitic Steel Surface Having a Fracture Stress of 15000 psi ($\sim$1.034 (10^8) N/m^2)

f	α, deg.	V_{ic}	
		in/s	m/s
0	90°	17.67	0.44
0	85°	17.60	0.44
0	65°	19.50	0.49
0	45°	25	0.63
0	20°	51.67	1.31
0	10°	101.78	2.58
0.25	90°	17.67	0.44
0.25	85°	0.49	$1.24(10^{-2})$
0.25	65°	0.55	$1.39(10^{-2})$
0.25	45°	0.7	$1.77(10^{-2})$
0.25	20°	1.45	$3.68(10^{-2})$
0.25	10°	8.62	$21.89(10^{-2})$
0.5	90°	17.67	0.44
0.5	85°	0.12	$3.04(10^{-3})$
0.5	65°	0.13	$3.30(10^{-3})$
0.5	45°	0.17	$4.31(10^{-3})$
0.5	20°	0.35	$8.89(10^{-3})$
0.5	10°	0.7	$17.78(10^{-3})$

Table 4. Magnitude of the Minimum Impact Velocity of Coal, Ash, and Slag Particles Required for the Cracking and Fragmentation of a Flat Martensitic Steel Surface Having a Fracture Stress of 30,000 psi ($\sim 2.068[10^8]$ N/m^2)

f	α, deg.	V_{ic}	
		in/s	m/s
0	90°	100	2.54
0	85°	100.3	2.54
0	65°	110.3	2.80
0	45°	141.4	3.59
0	20°	292.3	7.42
0	10°	575.7	14.62
0.25	90°	100	2.54
0.25	85°	2.82	$7.16(10^{-2})$
0.25	65°	3.10	$7.87(10^{-2})$
0.25	45°	3.97	$10.08(10^{-2})$
0.25	20°	8.21	$20.85(10^{-2})$
0.25	10°	16.18	$41.09(10^{-2})$
0.5	90°	100	2.54
0.5	85°	0.68	$1.72(10^{-2})$
0.5	65°	0.75	$1.90(10^{-2})$
0.5	45°	0.96	$2.43(10^{-2})$
0.5	20°	1.99	$5.05(10^{-2})$
0.5	10°	3.93	$9.98(10^{-2})$

the resulting sliding frictional shearing stresses intensify the surface tensile stresses. The results also indicate that the impact velocity required for fracturing decreases as the impact angle increases, and attains its smallest value at an impact angle slightly less than 90°. These results and the fact that V_{ic} has a jump discontinuity at 90° strongly suggest that a brittle solid would experience the largest amount of material loss due to erosion when the solid particles impact it at an angle that is slightly less than 90° but sufficiently large so as to allow the frictional shearing stresses to fully develop and attain their maximum limiting values.

The analysis shows that the surface tensile stresses, developed as a result of the eroding particles obliquely impacting a surface, greatly increases as the friction coefficient increases. In addition, the analytical results indicate that with sliding friction arising due to oblique impact of the eroding particles the normal stresses acting in the surface of contact are tensile at the leading edge of the contact surface and compressive at the rear; and that the surface tensile stresses at the leading edge are no longer radial. These findings would indicate that the Hertzian ring crack, which develops when the particles impinge at an angle of 90°, becomes broken and discontinuous in case of oblique impact. These results would suggest that if the particles impinge at an angle <90° so as to give rise to sliding frictional resistance between the eroding particles and a brittle surface, then the surface cracks and hence the fragments that eventually detach should be crescent-shaped.

Moreover, the conclusions and the numerical results strongly suggest that in an erosive environment where relative sliding takes place between the erosive particles and the surface of a brittle solid, the speed of impact required to cause fracture and fragmentation of the brittle solid decreases with increasing frictional resistance. It appears, then, that the formation of surface films

that can effectively reduce the frictional resistance should markedly reduce the amount of material loss due to erosion, abrasion, or adhesion. These conclusions should be most relevant in designing brittle solid members to withstand an erosive or abrasive environment such as that of a coal gasifier.

References

1. Division of Fossil Energy, Second Quarterly Report for January-March 1975.

2. Division of Fossil Energy, Third Quarterly Report for April-June 1975.

3. M. Mamoun, "On the Theories of Friction of Solids, Parts I, II, and III," ASME Papers 75-DE-8, -9, and -10, April 21-24, 1975.

Task F) Component Performance and Failure Analysis

(Principal Investigators: S. Greenberg and K. Natesan)

1. Hygas Pilot Plant

a. Instrument Tubes

The detailed metallographic analysis of the failed instrument tube is nearing completion and the final report is in preparation. The results support the originally stated conclusion that the observed failures (mixed transgranular and intergranular cracking) were associated with stress-corrosion cracking resulting from the exposure of Types 304 and 316 stainless steel to steam generated from water containing cloride.

Process pipe of the same composition as the instrument tubes and exposed to a similar but not identical environment has been subjected to extensive non-destructive and metallographic analysis. There is no evidence of failure but the plant operator has been made aware of the potential for failure and samples of process pipe will be examined at intervals in the future.

As a result of the investigation of this failure it was recommended that Incoloy 800 or Inconel 600 be used for instrument tubes exposed to superheated steam. The plant operator replaced the 18-8 stainless steel with Incoloy 800 and those tubes performed satisfactorily (i.e., no failures) during a recent successful run of 370 hours.

b. Thermocouple Sheath

The composition of the gas to which the Inconel 702 thermocouple sheath was exposed has been received from the plant operation and is in Table I. The explanation previously given, that failure was caused by internal oxidation, is consistent with the composition of the gas. The final report of this investigation is nearing completion.

As a result of the investigation of this failure, it was recommended that the thermocouple sheaths be fabricated of Type 310 stainless steel or nickel-base alloys containing >20% chromium. The plant operator replaced the Inconel 702 thermocouple sheaths with Type 310 stainless steel thermocouple sheaths and these sheaths performed satisfactorily (i.e., no failures) during the run indicated in (a).

Table I. Gas Composition

Gas	Vol. Percent*
H_2	20
H_2O	50-51
CO	9-12
CO_2	15-17
CH_4	2
H_2S	∿0.1

*At room temperature.

2. Synthane Pilot Plant

Welded process piping systems were specified, in general (with the exception of a high pressure steam system) to be constructed of carbon steel. The high pressure steam system was to be constructed of carbon-molybdenum and chromium-molybdenum steel. Throughout the piping systems there are instances of each of the three steels being inadvertently substituted for each of the three others.

Carbon steel is not suitable for the high pressure steam system because of the operating temperature. In some cases, piping of other than specified composition may be suitable. However, welding chromium-molybdenum steel using carbon steel welding procedures could produce cracked weldments in the heat affected zones due to the air-hardening characteristics of the chromium containing steel.

Six welded assemblies have been received for examination. Material is tentatively identified on the basis of visual observation of grinding sparks. Final identification will be on the basis of chemical analyses now in progress.

All welded assemblies were subjected to two-position X-ray examination. No cracks were detected. Ultrasonic examination of unground welds did not produce conclusive evidence of cracks. Based on the tentative alloy identification, three chromium-molybdenum to carbon steel welds were scheduled for metallographic examination. Examination of the first sample revealed the presence of a crack in the weld metal, apparently starting at the outside surface and penetrating at least 80% of the weld thickness.

Based upon these results it is recommended that all welded joints including nonspecified chromium-molybdenum steel be subjected to appropriate nondestructive examination techniques (if practicable). Cracked welds would be removed from the system and replaced with specified materials. Uncracked welds would be heat treated (250°F for 1 hr and air cooled - using electric heaters). The adequacy of the heat treatment would be determined by hardness measurement. Acceptable heat treatment results in Brinnell hardness of 200 or less. If the nondestructive testing outlined above cannot be carried out, then it is recommended all welds including nonspecified chromium-molybdenum steel be removed and replaced with specified materials.